HHS Public Access

Author manuscript

Neuron. Author manuscript; available in PMC 2018 February 08.

Published in final edited form as:

Neuron. 2017 February 08; 93(3): 646–660.e5. doi:10.1016/j.neuron.2016.12.037.

Optogenetic control of synaptic composition and function

Brooke L. Sinnen[1,*], **Aaron B. Bowen**[1,*], **Jeffrey S. Forte**[1,*], **Brian G. Hiester**[1,*], **Kevin C. Crosby**[1], **Emily S. Gibson**[1], **Mark L. Dell'Acqua**[1], and **Matthew J. Kennedy**[1,2,#]

[1]Department of Pharmacology, University of Colorado School of Medicine

Abstract

The molecular composition of the postsynaptic membrane is sculpted by synaptic activity. During synaptic plasticity at excitatory synapses, numerous structural, signaling and receptor molecules concentrate at the postsynaptic density (PSD) to regulate synaptic strength. We developed an approach that uses light to tune the abundance of specific molecules in the PSD. We used this approach to investigate the relationship between the number of AMPA-type glutamate receptors in the PSD and synaptic strength. Surprisingly, adding more AMPA receptors to excitatory contacts had little effect on synaptic strength. Instead, we observed increased excitatory input through the apparent addition of new functional sites. Our data support a model where adding AMPA receptors is sufficient to activate synapses that had few receptors to begin with, but that additional remodeling events are required to strengthen established synapses. More broadly, this approach introduces the precise spatiotemporal control of optogenetics to molecular control of synaptic function.

ETOC blurb

Sinnen et al. developed an approach to rapidly control the molecular composition of the postsynaptic density with light. Adding neurotransmitter receptors to the PSD had surprising functional effects that support a requirement for precise receptor positioning within PSD subdomains.

Introduction

At excitatory synapses throughout the central nervous system, the molecular composition of the postsynaptic membrane is a key determinant of synaptic strength. The repertoire and abundance of postsynaptic molecules are largely defined by the history of synaptic activity

[#]Correspondence: matthew.kennedy@ucdenver.edu, University of Colorado School of Medicine, Department of Pharmacology, P18-6103 MS8303, Aurora, CO 80045, ph: 303-724-3638, fax: 303-724-3663.

[2]Lead Contact

[*]Equal contribution

Author Contributions

Conceptualization, M.K.; Investigation, M.K., B.S, B.H., A.B., J.F., K.C.; Writing-Original Draft, M.K.; Writing-Review and Editing, B.S, B.H., A.B. M.D.; Supervision: M.K., M.D.; Funding Acquisition: M.K., M.D.

(Luscher et al., 2000; O'Brien et al., 1998; Shen and Meyer, 1999; Shi et al., 1999; Turrigiano et al., 1998). For example strong synaptic activation triggers accumulation of key signaling molecules at the postsynaptic density (PSD), a compact meshwork of scaffold molecules that anchors neurotransmitter receptors apposed to presynaptic release sites (Keith et al., 2012; Shen and Meyer, 1999). Downstream signaling events culminate in synaptic growth and addition of AMPA-type glutamate receptors to the PSD (Granger et al., 2013; Hayashi et al., 2000; Kauer et al., 1988). Similarly, prolonged synaptic inactivity also leads to a homeostatic increase in synaptic AMPA receptors (O'Brien et al., 1998; Turrigiano et al., 1998). AMPA receptors mediate most excitatory neurotransmission and it is thought that even subtle changes in the number of synaptic AMPA receptors could have a large effect on synaptic strength and neural connectivity. In the most extreme case, AMPA receptors are added to pre-formed, but non-functional synapses that initially contain few or no functional AMPA receptors giving the appearance of *de novo* synaptic connections (Durand et al., 1996; Isaac et al., 1995; Liao et al., 1995). Whether adding AMPA receptors to the PSD is sufficient to activate nascent connections, or to strengthen functionally mature synaptic connections in the absence of additional signaling and synapse growth normally accompanying plastic changes remains unknown. Furthermore, it is also unclear how the precise positioning of receptors *within* the PSD, relative to presynaptic neurotransmitter release sites, can influence responsiveness to neurotransmitter. Indeed, recent studies have demonstrated that the PSD is a heterogeneous structure, with different postsynaptic scaffold complexes organizing neurotransmitter receptors into distinct "nanodomains" within the PSD (MacGillavry et al., 2013; Nair et al., 2013; Tang et al., 2016). These observations suggest that synaptic transmission may not be sensitive to the overall number of receptors within the larger PSD, but rather their density within nanodomains positioned near presynaptic release sites. However, experimentally testing whether synaptic strength directly scales with receptor number has been challenging due to the lack of methodology for acutely manipulating the abundance of receptors within the PSD.

In addition to AMPA receptors, many other molecules are recruited to postsynaptic compartments during learning events that are important for synaptic plasticity. These include Ca^{2+}/calmodulin dependent protein kinase II (CaMKII) (Halt et al., 2012; Shen and Meyer, 1999), AKAP79/150 (Keith et al., 2012) and proteasome subunits (Bingol and Schuman, 2006) among others. Whether recruitment of any one, or combination of these factors in the absence of synaptic stimulation is *sufficient* to trigger functional changes associated with plasticity remains a fundamental but unresolved issue. Thus, new tools to conditionally tune the molecular composition of the PSD, on a rapid timescale, with fine spatial precision would be extremely valuable for dissecting the origins of enduring synaptic plasticity at the molecular scale, and could ultimately be used to manipulate circuit dynamics and excitation/inhibition balance in real time *in vivo* with unparalleled spatiotemporal precision.

Here we describe a novel approach to control the molecular composition and function of excitatory synapses with light, using an optical dimerization system based on the *Arabidopsis thaliana* photoreceptor cryptochrome 2 (CRY2) and its light-dependent interaction partner, CIB1 (Kennedy et al., 2010a). Using this system, we can rapidly, reversibly and locally control the level of nearly any protein at the postsynaptic membrane. To demonstrate the utility of our approach, we used our system to optically recruit AMPA-

type glutamate receptors to the PSD, which rapidly increased synaptic coupling. Surprisingly, enhanced coupling was primarily the result of an apparent increase in the number of functional synaptic connections, rather than strengthening of existing, functional connections. Potentiating synaptic stimuli delivered before light exposure occluded the functional effects of light-triggered receptor recruitment, demonstrating that artificially recruited receptors occupy the same sites as activity-recruited receptors. Our data support a model where receptor recruitment is sufficient to activate synaptic sites that had few or no receptors to begin with. In contrast, at established synapses, strength does not strictly scale with the number of PSD-localized receptors. Thus, in addition to receptor recruitment, distinct remodeling events that are normally engaged by plasticity stimuli are required to potentiate established synapses, perhaps by concentrating receptors in nanodomain structures within the PSD. More broadly, this novel approach introduces the spatiotemporal precision of optogenetics to molecular control of cellular microdomains.

Results

A general strategy for optogenetic manipulation of synaptic composition

We sought to engineer a system that would allow us to use light to manipulate the subcellular localization of proteins that normally accumulate in postsynaptic compartments during important forms of plasticity. Our system relies on the optical dimerizer pair CRY2/CIB1, which enables light-dependent dimerization of attached target proteins (Kennedy et al., 2010a). We anchored CRY2 at the postsynaptic membrane by fusing it to different PSD scaffold molecules, thus allowing recruitment of CIB-fused target proteins to the PSD (Fig. 1A). To concentrate CRY2 at the PSD, we tested CRY2 fusions with homer1c, PSD95, and a genetically-encoded “fibronectin intrabody generated with mRNA display” (FingR) that tightly binds to endogenous PSD95 ($PSD95_{FingR}$) (Fig. 1B) (Gross, 2013). All of the CRY2 fusion proteins localized to dendritic spines in dissociated hippocampal cultures and organotypic hippocampal slices, indicating that CRY2 did not disrupt their normal subcellular localization (Fig. 1B). To demonstrate that CRY2 remains functional when fused to PSD scaffold proteins, we visualized the localization of mCherry (mCh) fused to a truncated domain of CIB1 containing amino acids 1–170 (CIB-mCh) in dissociated hippocampal neurons before and after blue light exposure (Fig. 1C). In the dark, CIB-mCh filled the cell and showed no enrichment at synapses. Following blue light stimulation, we observed rapid recruitment of CIB-mCh to dendritic spines when using homer1c, PSD95 or $PSD95_{FingR}$ as CRY2 synaptic anchors. Data for CIB-mCh recruitment to CRY2-GFP-homer1c, ($\tau_{recruitment}$=0.52 min) is shown in Fig. 1C,D.

To quantify reversibility of the system, we stimulated neurons expressing CRY2-GFP-homer1c and CIB-mCh with a single pulse of blue light. CIB-mCh quickly accumulated and then dissociated from the PSD at a rate nearly identical to that previously reported ($\tau_{reversal}$=5.1 min) 6 (Fig. 1D) (Kennedy et al., 2010a). Following spontaneous reversion to its dark state, CRY2 can be repeatedly excited with subsequent light exposures (Fig. 1D). Thus target proteins can be recruited to the PSD for relatively short time periods (90% dissociation by 12min) or prolonged time periods (hours to days), depending on the frequency and duration of blue light exposure. We next compared the properties of light-

triggered PSD recruitment with synaptic activation-triggered recruitment. Ca^{2+}/calmodulin-dependent protein kinase II (CaMKII) exhibits robust translocation to postsynaptic sites upon NMDA receptor activation, a process that is critical for long term potentiation (LTP) (Halt et al., 2012; Shen and Meyer, 1999). We measured the extent and kinetics of CIB-mCh-CaMKII synaptic accumulation following NMDA receptor activation (with no blue light), or triggered with blue light exposure (with NMDA receptors blocked). Stimulating NMDA receptors with a "chemical LTP" (cLTP) protocol (Lu et al., 2001) resulted in robust CaMKII recruitment to dendritic spines within seconds (Fig. 1E). When we photoexcited neurons expressing CRY2-GFP-homer1c and CIB-mCh-CaMKII with blue light, we observed a nearly identical rate and extent of CaMKII accumulation in spines (Fig. 1E). Finally we demonstrate that PSD-localized CRY2 can be used to quickly, robustly, locally and reversibly photo-localize important synaptic proteins to postsynaptic compartments.

Recruiting neurotransmitter receptors to synapses with light

Diverse forms of synaptic plasticity rely on postsynaptic mechanisms that converge on the number of AMPA-type glutamate receptors at the postsynaptic membrane. However, whether simply adding receptors to the PSD is sufficient to strengthen synapses, or whether additional pre- and postsynaptic remodeling events are also required remains a fundamental question due to the lack of methodology for conditionally titrating receptors into the PSD, absent the myriad molecular signaling events that accompany plasticity stimuli. We engineered our system to directly add AMPA receptors to the postsynaptic membrane by fusing CIB to the AMPA receptor subunit GluA1 at its intracellular C-terminus. To visualize receptors we fused a red fluorescent protein (mCh or mOr2) fused to either the extracellular (N-terminal) or intracellular C-terminal domain, between CIB and GluA1 (mCh/mOr-GluA1-CIB and GluA1-mCh-CIB) (Fig. 2A). Prior to light exposure, surface localization and spine enrichment of CIB-tagged GluA1 receptors were identical to expressed receptors without the CIB tag and similar to endogenous GluA1 and GluA2 (Fig. S1A–D). Upon light stimulation, we observed robust and rapid GluA1 accumulation in dendritic spines (Fig. 2B, Movie S2). The rate of AMPA receptor translocation to synaptic sites was slower than for soluble proteins, but still occurred on a rapid timescale ($\tau_{GluA1\text{-}CIB}$=3.3 min vs. $\tau_{CIB\text{-}mCh}$=0.52 min) (Fig. 2C), presumably due to slower diffusion in the plasma membrane and steric hindrance within the synaptic cleft. The kinetics of light-triggered GluA1-CIB accumulation were nearly identical to GluA1 recruited to the PSD by synaptic stimulation using the same cLTP protocol we used for CaMKII PSD recruitment (see Methods) (Figs. 2C). To confirm that light-recruited receptors were on the spine surface, we engineered a thrombin cleavage site between mCh and GluA1. Treatment with thrombin following synaptic accumulation eliminated >80% of the spine mCh signal, confirming surface expression of recruited receptors (Fig. S1E).

We next tested whether CRY2/CIB recruitment of AMPA receptors to postsynaptic sites led to persistent synaptic localization of receptors beyond the lifetime of the CRY2/CIB interaction. That is, is recruiting receptors to synapses for a short time period sufficient for enduring changes in synaptic composition? Our system is ideally suited for this question

since the CRY2/CIB interaction decays with a time constant of ~5 min. Thus ~95% of photoexcited CRY2 will have dissociated from CIB after 15 min. This is a major advantage over previously developed chemical-induced dimerization strategies (Spencer et al., 1993), which are essentially irreversible on the timescale of most experiments. We recruited GluA1-mCh-CIB to postsynaptic sites labeled with CRY2-GFP-homer1c, followed by an extended dark recovery period. Following synaptic accumulation, GluA1-CIB fully dissociated from the majority of synapses (Fig. 2D). The rate of GluA1-CIB dissociation ($\tau_{reversal}$=12.5 min) from PSDs was ~2.5-fold longer than the lifetime of the photoexcitated (CIB-bound) state of CRY2 in the PSD, measured under identical conditions ($\tau_{reversal}$=5.1 min) (Fig. 2D). Thus, the lifetime of the CRY2/CIB interaction is not rate-limiting for GluA1 exit from the PSD. Instead, GluA1 exit appears to be limited by diffusional trapping mediated by interactions with native PSD components. In our experiments, we exposed neurons to a single pulse of blue light every 2–3 min. Thus, following initial PSD recruitment, a significant fraction of GluA1-CIB will have dissociated from CRY2 between light pulses (~50% after 3 min) but most dissociated receptors will remain trapped within the PSD.

We next determined whether translocation and dissociation properties were influenced by the identity of the postsynaptic scaffold to which the receptors were recruited. We first used photoactivation light microscopy (PALM) (Betzig et al., 2006) and direct stochastic optical reconstruction microscopy (dSTORM) (Heilemann et al., 2008; Rust et al., 2006) to localize the different scaffolds used in this study. Figure 2E shows several synapses where PSD95 was localized using $PSD95_{FingR}$-mEOS and CRY2-GFP-homer1c was localized using anti-GFP (detected with Alexa647). We used a Density-Based Clustering of Applications with Noise (DBSCAN) algorithm (Ester et al., 1996) to define clusters of PSD95 and then calculated the fraction of overlapping homer1c in individual dendritic spines. We observed that homer1c and PSD95 occupied largely overlapping, but somewhat distinct subdomains within dendritic spines, consistent with previous reports (Dani et al., 2010; Tang et al., 2016). On average, 62.6±0.03% (n=93 spines from 6 neurons) of spine homer1c localizations overlapped with PSD95 clusters. Consistent with their similar spine localization, we found that the rates of light-triggered GluA1-CIB association and dark dissociation were indistinguishable when recruited to the PSD via CRY2-GFP-homer1c or CRY2-$PSD95_{FingR}$ (Fig. 2F).

Recruited receptors infiltrate the PSD

Because our approach relies on an artificial protein interaction to recruit receptors to the PSD, it is possible that receptors do not fully access the PSD either through steric interference or because the CRY2-fused scaffolds do not fully decorate the PSD. To confirm that recruited receptors are able to penetrate the PSD, we used PALM/dSTORM to more precisely localize GluA1 receptor position in dendritic spines relative to the endogenous PSD95. Using this approach we first compared the PSD distribution of expressed GluA1-CIB to endogenous GluA1. For these experiments, we used photoswitchable GluA1-mEOS-CIB (red channel), along with either CRY2-GFP-$PSD95_{FingR}$ or CRY2-GFP-homer1c to recruit GluA1 to synaptic sites and an antibody to detect endogenous PSD95 (far red channel). We used an antibody against an extracellular epitope of GluA1 to label native

AMPA receptors (Kennedy et al., 2010b). We calculated the number of GluA1 localizations within the PSD, defined using a DBSCAN clustering algorithm (see methods), and divided this value by the total number of localizations within each spine. Figure 3A shows representative PALM/STORM data for endogenous GluA1 relative to endogenous PSD95. We observed a broad distribution of PSD occupancy for both endogenous and expressed GluA1-CIB, with some synapses displaying few overlapping localizations while others on the same dendritic branch displayed a high degree of overlap (Fig. 3A–D). Figure 3B shows representative synapses with high and low degrees of GluA1/PSD overlap for endogenous and expressed receptors. Figure 3C shows examples of the DBSCAN method for defining the PSD and calculating the fraction of receptors within the PSDs of individual dendritic spines. We observed a nearly identical synaptic (PSD-overlapped) GluA1 distribution between endogenous GluA1 and expressed GluA1-CIB in dark-treated cells (Fig. 3D). On average, 40±3% of endogenous GluA1 spine localizations overlapped with the PSD compared to 43±3% for GluA1-mEOS-CIB in dark-treated cells. To test if light treatment increased the fraction of GluA1-CIB receptors within the PSD, we compared the fraction of PSD-localized signal for dark- and light-treated neurons. In light-treated cells expressing GluA1-CIB and CRY2-PSD95$_{FingR}$, the distribution of PSD-localized GluA1-CIB robustly shifted toward higher PSD occupancy (Fig. 3D). Figure 3E shows a scatter plot summary of the data comparing dark and light treated cells expressing GluA1-CIB along with either CRY2-homer1c or CRY2-PSD95$_{FingR}$. Recruiting GluA1-CIB to either scaffold led to a robust increase in AMPA receptor occupancy within the PSD. Thus, not only does light increase the overall number of GluA1-CIB receptors in spines (based on our live cell confocal imaging experiments, Fig. 2D), but it also concentrates spine receptors within the PSD.

Functional enhancement of excitatory synaptic input with light

After establishing that recruited receptors access the PSD, we next tested whether adding AMPA receptors to the PSD influences synaptic function. For these experiments, we used CRY2-PSD95$_{FingR}$ to avoid the potential for perturbing basal synaptic function by overexpressed PSD scaffolds. We biolistically transfected organotypic hippocampal slices with CRY2-PSD95$_{FingR}$-GFP and GluA1-mCh-CIB. Whole cell recordings were performed on CA1 pyramidal neurons expressing these constructs 36–48 hours following transfection. Schaffer collaterals were stimulated at 0.1 Hz during a 5–10 min baseline period, before the slice was exposed to blue light (2 sec pulse every 2–3 min) (Fig. 4A). In 9 out of 11 cells, we observed an increase in evoked EPSC amplitude within 15 min of blue light exposure (Fig. 4A–B). The time course of EPSC potentiation is plotted for a single representative cell (raw EPSC values) and for averaged, compiled data in Figure 4A. Following light exposure, evoked EPSC amplitude increased at a rate similar to GluA1-CIB recruitment (τ=4.5 min vs. 3.3 min respectively) measured in dissociated hippocampal neurons. Control cells expressing tdTom instead of GluA1-mCh-CIB, demonstrated no change in evoked EPSC amplitude upon blue light exposure (Fig. 4B).

Enhanced synaptic coupling is due to an increase in the apparent number of functional synapses

Enhanced synaptic coupling can occur through strengthening existing synapses, and/or increasing the number of functional synapses. To begin distinguishing these possibilities, we measured evoked quantal responses from CA1 pyramidal neurons in organotypic hippocampal slices in the presence of 4 mM Sr^{2+}, which favors asynchronous release of neurotransmitter vesicles following electrical stimuli. This method allows us to measure evoked, asynchronous EPSCs (aEPSCs) arising from quantal neurotransmitter release (Bekkers and Clements, 1999). Figure 4C shows twenty representative sweeps (200 ms in duration) before and after blue light exposure from CA1 pyramidal neurons expressing GluA1-mCh-CIB and CRY2-$PSD95_{FingR}$-GFP. In control sweeps, where no electrical stimulus was delivered, spontaneous EPSCs were rare, indicating that the majority of the events we observed were triggered by the stimulus (Fig. 4C). Surprisingly, we observed no change in the average aEPSC amplitude or cumulative distribution after blue light exposure, even in cases where the aggregate EPSC (which typically peaked 4–10 ms following stimuli under these conditions) grew larger (Fig. 4D, E).

With no observable change in quantal amplitude, we next tested whether more quantal events were elicited following the same stimulus, which would reflect the generation of new functional connections. We counted the number of quantal events triggered by evoked stimulation under asynchronous release conditions (1 mM Ca^{2+}/4mM Sr^{2+}) in a time window 50–200 msec following stimulation from 50 consecutive sweeps recorded in the dark, and in the same cells 4–10 min following blue light exposure (Fig. 4F). Following light exposure, we observed an increase in the total number of events, suggesting that receptor recruitment increases the number of functional synaptic sites rather than potentiating existing synapses.

As an independent method of investigating whether receptor recruitment influences quantal amplitude and/or frequency, we also measured miniature EPSCs (mEPSCs) in dissociated hippocampal neurons expressing GluA1-mCh-CIB along with CRY2-GFP-homer1c, CRY2-$PSD95_{FingR}$-GFP, or PSD95-GFP-CRY2. mEPSCs were recorded over a 2 min baseline period in the dark, and then at various times up to 20 min following blue light exposure (Fig. 5A). Consistent with our aEPSC results, we observed little difference in the average values or cumulative distribution of mEPSC amplitudes following receptor recruitment to any of the three CRY2-PSD scaffolds tested (Fig. 5B–E). Instead, we observed a consistent elevation in mEPSC frequency (1.6 ± 0.19 fold over background 4–6 min following illumination for CRY2-GFP-homer1c, n= 14 cells) (Fig. 5E). Increased mEPSC frequency occurred with nearly identical kinetics as receptor recruitment to the PSD (mEPSC enhancement τ=3.4 min vs. receptor recruitment τ=3.3 min) (Fig. 5F). Neither mEPSC frequency nor amplitude increased over the same time period in control cells expressing CRY2-GFP-homer1c and CIB-mCh (Fig. 5E).

Increased quantal frequency is often interpreted as increased synapse number, or increased probability of neurotransmitter release. Indeed, AMPA receptor-dependent retrograde signaling to 13 presynaptic neurotransmitter release mechanisms and synaptogenic processes have been reported (Lindskog et al., 2010; Ripley et al., 2011; Tracy et al., 2011). To test if

recruited GluA1 influences presynaptic properties, we loaded FM4-64 into presynaptic terminals contacting hippocampal neurons expressing mCh-GluA1-CIB and CRY2-GFP-homer1c in the dark (Fig. S2A). We then either exposed the neurons to pulses of blue light over a period of 10 min to recruit GluA1-CIB to postsynaptic sites, or kept the cells in darkness followed by depolarization-induced FM4-64 unloading (Fig. S2B). We observed no change in the rate of FM dye unloading at presynaptic terminals apposed to postsynaptic sites with light-recruited GluA1 vs dark-treated cells. Because our mEPSC measurements were made under spontaneous release conditions (1 μM TTX), we also measured the rate of spontaneous neurotransmitter release with an independent method that reports spontaneous quantal release. Using the genetically encoded Ca^{2+} indicator jRGECO1a expressed in postsynaptic neurons (along with SEP-GluA1-CIB and untagged CRY2-homer1c), we can observe Ca^{2+} entry through activated NMDA receptors in response to spontaneous quantal neurotransmission (Dana et al., 2016; Sinnen et al. 2016). Thus we can quantify the frequency of spontaneous neurotransmitter release events at the same synaptic sites before and after GluA1 recruitment. Consistent with our FM4-64 experiment, the rate of spontaneous release was not sensitive to GluA1 recruitment, (Fig. S2C,D). Finally, spine number was also identical before and after GluA1 recruitment ruling out new spine sprouting as a mechanism for increased quantal frequency (Fig. S2E). Together, these data strongly suggest that the functional effects we observe are a result of postsynaptic modification of the PSD.

Activity-driven GluA1 recruitment occludes light-recruitment functional effects

With no observable change in presynaptic properties, we focused our attention on GluA1 recruitment to postsynaptic sites as the mechanism for the apparent increase in synaptic connectivity. One explanation for this result is that recruited AMPA receptors are able convert weak or silent synapses (that initially lack AMPA receptors) into functional connections. Consistent with this, we observed a significant fraction of synapses with sparse (<20% of total spine localizations) GluA1 PSD occupancy under basal conditions (Fig. 3A–C). This value drops from 23% in the dark to 8% following light recruitment to homer1c and from 30% to 15% following recruitment to PSD95 (Fig. 3D,E). However because it is impossible to ascertain whether these sparsely labeled synapses represent non-functional connections, we wanted further functional evidence. If this hypothesis is true, then activating silent synapses using synaptic activity to drive AMPA receptors into synaptic sites should occlude the effects of light recruitment. Indeed, there is strong evidence that synaptic stimulation recruits AMPA receptors to postsynaptic sites to both strengthen established synapses and to activate silent or weak synapses that initially lacked AMPA receptors (Kerchner and Nicoll, 2008). For example, global “chemical LTP” (cLTP) stimulation results in increased mEPSC amplitude and an even more robust increase in mEPSC frequency, consistent with conversion of silent synapses to functional contacts through AMPA receptor recruitment (Gu et al., 2010; Keith et al., 2012; Lu et al., 2001). Thus, if GluA1-CIB is recruited to silent synaptic sites that normally recruit receptors in response to synaptic activity, cLTP should occlude the functional effects of artificial recruitment.

For these experiments, we pretreated neurons expressing CRY2-GFP-homer1c and GluA1-mCh-CIB in the dark with an established cLTP paradigm (4 min exposure to a solution

containing 200μM glycine, 0mM Mg^{2+} and 30μM bicuculline) that triggers AMPA receptor translocation to 15 synaptic sites and a reliable increase in mEPSC frequency and amplitude. To verify the cLTP stimulus recruited AMPA receptors to spines, we visualized AMPA receptors in live neurons with either mCh-GluA1-CIB or SEP-GluA1. Following cLTP, we observed a robust increase in both mCh-GluA1-CIB and SEP-GluA1 fluorescence in dendritic spines (Fig. S3). These data also show that C-terminally CIB-tagged receptors exhibit normal activity-triggered synaptic trafficking (Fig. S3). We next recorded mEPSCs before and after light exposure to assess whether light recruitment was additive with or occluded by prior cLTP treatment (Fig. 6A). Interleaved cells not exposed to cLTP served as a positive control for the effectiveness of light-recruitment of GluA1-CIB. cLTP stimulus alone increased mEPSC frequency to a value indistinguishable from that observed following light recruitment of GluA1-mCh-CIB alone (2.4 ±0.35 Hz baseline; 3.5±0.42 Hz cLTP alone, 3.3±0.40 Hz light recruitment alone)(Fig. 6B). Importantly, prior cLTP stimulus completely occluded further mEPSC frequency enhancement by light-induced GluA1 recruitment (3.5±0.42 Hz cLTP alone; 3.6 ±0.4 Hz cLTP followed by light recruitment, p=0.69 paired Student's t-test) (Fig. 6B). cLTP stimulation alone increased mEPSC amplitude from 13.3±0.5 pA to 15.4±0.9 pA (p=0.03, Student's t-test) consistent with other reports, but as in our previous experiments, light treatment had no further effect on mEPSC amplitude following cLTP (post/pre-light mEPSC amplitude=0.91±0.04). We also measured whether GluA1-CIB recruited to the PSD by synaptic stimulation occluded further recruitment by light. We first exposed cells to cLTP stimulus to recruit GluA1, and then exposed the cells to light. We found that prior cLTP significantly impaired further PSD recruitment by light (Fig. S3C). Combined with our super resolution imaging experiments, these data provide strong evidence that artificially recruited receptors access the PSD to occupy the same sites as receptors recruited by synaptic activity.

Evidence for functional organization of AMPA receptors within the PSD

We next investigated why quantal amplitude does not scale up following receptor recruitment, even though recruited receptors infiltrate the PSD (Fig. 3). Given the low affinity of AMPA receptors for glutamate, models of quantal synaptic transmission restrict postsynaptic AMPA receptor activation to subsynaptic "hotspots" ~250 nm in diameter apposed to presynaptic vesicle release sites (Franks et al., 2003; Raghavachari and Lisman, 2004). These models are supported by functional experiments showing non-saturation of synaptic AMPA receptors by quantal release and imaging experiments revealing that AMPA receptors are organized in nanoscale clusters within the PSD near presynaptic neurotransmitter release sites (MacGillavry et al., 2013; McAllister and Stevens, 2000; Nair et al., 2013; Tang et al., 2016). Thus, synaptic strength could be more sensitive to the number of receptors localized within these hotspots, not by the total number of receptors housed in the PSD (Fig. 7A). If this is the case, then flooding the PSD with additional receptors may have little effect on quantal amplitude if the density of receptors within postsynaptic "hotspots" remains unperturbed. Our observation that quantal amplitude remains unchanged in the face of increased PSD-localized GluA1 is consistent with this model. To provide additional evidence, we performed an experiment where we enlarged the radius of AMPA receptor activation by artificially introducing glutamate by uncaging MNI-glutamate over single spines. Because the exact location of vesicular neurotransmitter

release is impossible to replicate with uncaging, and because the uncaging volume is limited by light diffraction (~300 nm in x/y dimension and ~1 μm in the z dimension using single photon uncaging) it is inevitable that receptors outside of natural "hotspots" will be activated. Thus, the amplitude of uncaging-evoked AMPA currents (μEPSCs) will be less sensitive to receptor clustering within PSD sub-structures and more faithfully reflect the *total* number of AMPA 17 receptors in the PSD. For these experiments, we used dissociated hippocampal neurons expressing CRY2-GFP-homer1c along with either mCh-GluA1-CIB or CIB-mCh as a control. The uncaging laser intensity was tuned such that the recorded μEPSCs amplitudes resembled mEPSC amplitudes. In separate neurons, we confirmed that uncaging-evoked responses were consistently confined to individual dendritic spines under these conditions by imaging NMDA receptor-mediated Ca^{2+} influx (Fig. S4A). In neurons expressing mCh-GluA1-CIB along with CRY2-GFP-homer1c, we observed a robust increase in μEPSC amplitude following blue light exposure but no change in mEPSC amplitude under identical conditions (Fig. 7B,C). On average, post-light μEPSCs increased by 1.5±0.1-fold over baseline responses for GluA1-CIB expressing neurons while control neurons expressing CIB-mCh displayed no change in average post-light μEPSC amplitude (Fig. 7C). To further prove that μEPSC responses were mediated by recruited GluA1-CIB receptors, we took advantage of the unique biophysical properties of expressed homomeric GluA1, which displays faster response kinetics and inward rectification. We observed faster μEPSC decay kinetics and robust inward rectification of μEPSC responses at synapses with recruited GluA1-CIB compared to control synapses with recruited CIB-mCh (Fig. S4B,C). Taken together, these experiments provide evidence for functional organization of receptors within the PSD. These experiments also confirm that CIB-tagged receptors are functional following recruitment to the PSD, eliminating possible concerns that the CIB-tag or the CRY2/CIB interaction may block receptor function.

Recruited receptors exchange with endogenous receptors at functional sites with no net change in quantal amplitude

We find that functional GluA1-CIB receptors are added to the PSD with no change in quantal amplitude. Thus, recruited receptors either do not have access to hotspots of activation within the PSD, or they are in equilibrium with endogenous receptors at these sites. To distinguish between these possibilities, we took advantage of the pharmacology of expressed GluA1 receptors, which are uniquely sensitive to the polyamine antagonist IEM1460. We compared the effects of IEM1460 on mEPSC parameters in dissociated hippocampal neurons expressing CRY2-GFP-homer1c and GluA1-CIB that were either kept in the dark or pre-treated with light. If recruited receptors cannot integrate into functional domains within the PSD, adding IEM1460 should not affect mEPSC amplitude (Fig. 7D). On the other hand, if recruited GluA1 is in equilibrium with endogenous receptors, IEM1460 should decrease mEPSC amplitude since at least a fraction of AMPA receptor current will be mediated by GluA1 (Fig. 7D). In both scenarios, IEM1460 will decrease mEPSC frequency since we previously demonstrated that a fraction of synapses contain predominantly GluA1-CIB receptors following light recruitment (Fig. 5). In control experiments, adding 50μM IEM1460 to untransfected cells had little effect on mEPSC frequency or amplitude, consistent with the majority of synaptic AMPA receptors containing the GluA2 subunit (Lu et al., 2009) (Fig. 7E,F). Likewise, we observed only a small

reduction in mEPSC frequency and amplitude in control cells expressing CRY2-GFP-homer1c and mCh-GluA1-CIB, but kept in the dark (Fig. 7F), demonstrating a modest level of GluA1-mCh-CIB synaptic incorporation prior to light treatment. As expected, adding IEM1460 to light-treated neurons caused a robust decrease in mEPSC frequency that precisely offset the frequency increase we observed when GluA1 was initially recruited to synapses (Fig. 7F). mEPSC amplitudes were reduced to a greater extent in light-than dark-treated neurons upon addition of IEM1460 (post-IEM1460 normalized to pre-IEM1460 baseline, dark cells = 0.94 ± 0.03; light-treated cells: 0.76 ± 0.03, p=0.001, Student's t-test) (Fig. 7F). Thus, a significant fraction of PSD-recruited GluA1-CIB homomers exchange with endogenous receptors at functional domains within the PSD. We next tested if the exchange between functional endogenous receptors and recruited GluA1-CIB takes place within spine subdomains, or if recruited receptors completely displace endogenous receptors from spines. We antibody-labeled endogenous GluA2-containing receptors in live hippocampal neurons and then recruited GluA1-CIB to the PSD while imaging antibody-labeled GluA2. We observed no reduction in spine GluA2 signal upon GluA1-CIB recruitment suggesting that any functional exchange that takes place occurs at spine subdomains with no net loss of endogenous receptors from spines (Fig. S4D).

Discussion

Using light to control biological processes has emerged as a powerful approach for experimentally addressing previously intractable problems. The explosion of opsin-based optogenetic tools for remote control of neural firing has already led to major advances in dissecting the neural circuitry for diverse behaviors in the relatively short time these tools have been available (Boyden et al., 2005). While the use of light-sensitive channels and pumps has been transformative, there remains an unmet need for molecular tools to precisely control other important aspects of neural function. Here we developed a new optogenetic approach to modify the molecular composition of the postsynaptic membrane, demonstrating for the first time that light can be used to rapidly tune excitatory synaptic connectivity.

Paradoxical functional effects of AMPA receptor recruitment

Perhaps the most surprising result of this study is the discovery that recruiting AMPA receptors to the postsynaptic membrane had little effect on the strength of most excitatory synapses (as measured by quantal amplitude) even though we observed robust receptor recruitment at the majority of dendritic spines. A trivial explanation is that the artificial interaction between CRY2 and CIB-tagged GluA1 receptors renders them non-functional and/or they do not have full access to the PSD. We believe this is not the case for multiple reasons. First, our super resolution imaging data demonstrate that recruited receptors infiltrate the PSD. Second, we see clear functional effects upon GluA1 recruitment (evoked EPSC potentiation and increased mEPSC frequency). Third, these functional effects are fully blocked by a selective GluA1 antagonist, confirming that they arise from recruited receptors. Fourth, uncaging evoked AMPA currents at single spines grow larger upon receptor recruitment, are inwardly rectifying and decay with faster kinetics, confirming GluA1-CIB function following PSD recruitment. Finally, prior AMPA receptor recruitment

to synaptic sites triggered by synaptic activity completely occludes functional effects of GluA1-CIB recruitment. Thus, using the CRY2/CIB system, we are adding functional AMPA receptors to the PSD yet quantal amplitude remains largely unperturbed. This observation is even more surprising considering that the homomeric GluA1 receptors we are recruiting to the PSD have higher single channel conductance than endogenous GluA2-containing receptors. However, this observation is not without precedent. Synaptic transmission is mediated solely by high-conductance GluA1 homomers in both conditional and constitutive GluA2/3 double knockout animals, yet quantal amplitude remains unchanged (Lu et al., 2009; Meng et al., 2003). In another example, synaptic transmission in mice harboring engineered AKAP79/150 with impaired calcineurin binding is primarily mediated by high-conductance, GluA2-lacking AMPA receptors, yet quantal amplitude is not altered (Sanderson et al., 2012). Thus, quantal amplitude appears to be tightly regulated through currently unknown mechanisms, even following rapid addition of functional AMPA receptors to the PSD, as shown here.

Our data is consistent with theoretical models proposing that precise “hotspot” localization of AMPA receptors within PSD subdomains near presynaptic neurotransmitter release sites is required for glutamate binding and activation (Lisman and Raghavachari, 2006; Raghavachari and Lisman, 2004). Indeed, previous functional studies showing non-saturation of postsynaptic AMPA receptors by quantal neurotransmission have been further supported by recent imaging experiments describing AMPA receptor clustering within PSD nanodomains, often apposed to presynaptic neurotransmitter release sites (MacGillavry et al., 2013; McAllister and Stevens, 2000; Nair et al., 2013; Tang et al., 2016). It is tempting to speculate that such nanodomains represent sites of functional neurotransmission, and that receptors outside of these clusters do not appreciably contribute, even though they localize to the PSD. Given the low affinity of AMPA receptors for glutamate, precise positioning of receptors vis-à-vis presynaptic neurotransmitter release sites could have a major impact on postsynaptic responses. Indeed, while receptor recruitment to the PSD did not influence quantal amplitude in response to naturally released glutamate, we did observe a robust increase in AMPA receptor responses when we bypassed natural neurotransmitter release by uncaging glutamate, which would be less sensitive to nanoscale positioning effects. This observation confirms we are adding functional receptors to the PSD and that increasing total receptor number within the PSD does not necessarily increase receptor number within sub-PSD domains responsible for natural neurotransmission. This was not the result of recruited receptors being excluded from functional domains within the PSD due to the artificial nature of recruitment, since our IEM1460 experiments show that recruited receptors are in equilibrium with endogenous receptors at functional sites within the PSD. We speculate that additional postsynaptic remodeling must occur during potentiating forms of plasticity, not only to recruit more receptors to the PSD, but also to concentrate them in the appropriate sub-PSD nanodomain.

While we did not observe increased quantal amplitude, we did observe a robust increase in the apparent *number* of functional synapses, measured by increased evoked and spontaneous quantal frequency. Numerous previous studies have demonstrated a robust increase in quantal frequency with a relatively modest change in amplitude following global LTP stimuli (Fitzjohn et al., 2001; Keith et al., 2012; Lu et al., 2001; Malgaroli and Tsien, 1992).

Early reports interpreted this observation as a presynaptic enhancement of neurotransmitter release (Malgaroli and Tsien, 1992; Malinow and Tsien, 1990), but more recent evidence supports the presence of “silent synapses” which are initially devoid of AMPA receptors (Isaac et al., 1995; Liao et al., 1995). Strong synaptic stimulation can drive AMPA receptors into these synapses, resulting in the appearance of new functional synaptic connections (Kerchner and Nicoll, 2008). While this topic has been somewhat controversial, our data provide additional support for conversion of silent synapses to functional connections through postsynaptic AMPA receptor recruitment but do not rule out the potential for additional presynaptic remodeling events following plasticity stimuli. Our data also do not rule out the possibility of multiple, independent postsynaptic hotspots for neurotransmission at individual synapses. Thus it is plausible that increased quantal frequency results from AMPA receptor incorporation into silent subdomains of already functional synapses.

AMPA receptor recruitment and plasticity

Our data show that simply adding receptors to the PSD of established synapses is not sufficient to drive potentiation, yet functionally mature synapses are able to undergo plasticity (Bagal et al., 2005; Matsuzaki et al., 2004; Zhang et al., 2008). For example, homeostatic scaling paradigms uniformly scale the amplitudes of quantal synaptic currents at all synapses (O’Brien et al., 1998; Turrigiano et al., 1998). Likewise during LTP, extrasynaptic AMPA receptors are recruited to and trapped at the PSD, suggesting that synaptic stimulation triggers the genesis of new binding sites, or “slots” for AMPA receptors (Opazo et al., 2012; Redondo and Morris, 2011). Using our approach, we are able to test whether simply driving AMPA receptors into the PSD, absent the numerous and complex remodeling events that normally accompany LTP and homeostatic scaling, is sufficient to increase synaptic strength. While our data provide evidence that receptor recruitment is sufficient to activate previously weak or silent connections, our data imply that additional remodeling events that normally accompany plasticity are required to potentiate functionally mature synapses, perhaps by concentrating recruited receptors in the appropriate PSD nanodomains.

Intriguing parallels to our observations have been observed during LTP, where a pool of AMPA receptors is first trafficked to synaptic or perisynaptic regions that does not initially participate in synaptic transmission until secondary processes integrate this cohort of receptors for full expression of LTP (Yang et al., 2008). Indeed, numerous biochemical signaling pathways are engaged during LTP that drive cellular processes important for postsynaptic function. For example, dendritic spines undergo robust growth following LTP stimuli that correlates with enhanced AMPA receptor current and PSD enlargement by actin remodeling and addition of new scaffold molecules (Bosch et al., 2014; Keith et al., 2012; Matsuzaki et al., 2004). These processes possibly concentrate receptors within existing functional hotspots or add new functional sites to established synapses (Lisman and Raghavachari, 2006). Additionally, post-translational modifications to existing synaptic AMPA receptors can increase their conductance and open probability (Banke et al., 2000; Benke et al., 1998), resulting in increased quantal amplitude without the need for additional receptors. Finally, retrograde signaling to presynaptic terminals through AMPA receptor extracellular domains has also been reported, raising the possibility that recruiting AMPA

receptors to postsynaptic sites could influence presynaptic release properties, or the generation of new release sites (Lindskog et al., 2010; Ripley et al., 2011; Tracy et al., 2011). While we observed no difference in presynaptic function in this study, it is possible that recruitment of different AMPA receptor subunits (e.g. GluA2-containing receptors), or delivering synaptic stimulation in addition to GluA1 recruitment could lead to retrograde presynaptic modulation.

Future directions

In summary, we have developed a method for photo-tagging postsynaptic sites that allows unprecedented spatiotemporal control of the PSD. We use this approach to study molecular remodeling events at the postsynaptic membrane. Acutely manipulating the PSD on a fast timescale allows concurrent functional measurements using sensitive imaging and/or electrophysiology approaches before, during and after light exposure in the same neuron, a major advantage over traditional approaches. We see future potential using this approach to acutely control the ratio of synaptic excitation and inhibition (E/I balance). E/I balance is disrupted in numerous neuropsychiatric disorders, yet no methods exist to directly manipulate this parameter at the synaptic level, in real time to experimentally link disruptions in E/I balance to disease-associated behavior. This technology should be adaptable for controlling the molecular composition of inhibitory synapses for bidirectional control of neural circuit dynamics. One major limitation for implementing our approach *in vivo* is the large size of the CRY2 photoreceptor and the two-component nature of the system, which has hampered packaging into viral vectors for facile use in animals. Nevertheless, we see future utility using our approach to control synaptic strength and circuit dynamics *in vivo* using knock-in mouse lines expressing CRY2-fused PSD modules, and delivering CIB-fused target proteins in a single virus. Because CRY2 is actuated by blue light, hardware developed for increasingly commonplace *in vivo* channelrhodopsin experiments could be easily repurposed for CRY2-based optogenetics. Thus, our approach will have broad utility at multiple levels, from precise control of molecular signaling events within synaptic nanodomains to manipulating neural circuit dynamics *in vivo* during behavior.

STAR METHODS

CONTACT FOR REAGENT AND RESOURCE SHARING

Further information and requests for resources and reagents should be directed to and will be fulfilled by the Lead Contact Matthew Kennedy, matthew.kennedy@ucdenver.edu

EXPERIMENTAL MODEL AND SUBJECT DETAILS

All animal procedures were carried out in accordance with a protocol approved by the University of Colorado Denver Institutional Animal Care and Use Committee. All dissociated and slice cultures were prepared from Sprague-Dawley rats. Timed pregnant dams (typically embryonic day 16) were obtained from Charles River Laboratories and housed under standard conditions. This study used slices and dissociated cultures from both male and female pups.

Organotypic and dissociated hippocampal cultures—Organotypic cultures and dissociated neurons were prepared from Sprague Dawley rats as previously described (Stoppini et al., 1991). Briefly, hippocampi were dissected from postnatal day 5–7 rat pups and 300 μm slices were cut using a McIlwain tissue chopper. Slices were plated on porous membrane inserts in 6 well plates. Dissociated hippocampal neurons were prepared from P0–P1 pups. Dissociated hippocampal neurons were transfected between 14 and 18 days *in vitro* (DIV) with lipofectamine 2000 according to the manufacturer's protocol. Microscopy and electrophysiology experiments were performed within 40–50 hours of transfection. Organotypic cultures, prepared from P5–P7 pups, were cultured for 7–10 days before biolistic transfection of CRY2/CIB plasmids. Whole cell patch clamp recordings were made within 40–50 hours following biolistic transfection (between 9 and 12 days *in vitro*). Biolistic transfection and gold particle preparation was carried out as described (Woods and Zito, 2008). Briefly, 1.6μm gold particles (Biorad, Cat #1652264) were coated with plasmid DNA. For CAG promoter constructs 1–2μg of DNA was used for 6–8mg of gold microparticles. For CamKIIalpha promoter constructs, we used 4–6μg of DNA for 6–8mg of gold. DNA coated gold particles were adsorbed onto Tefzel tubing (Biorad Cat #1652441) in anhydrous ethanol and then dried with a slow stream of nitrogen gas. Organotypic slices were bombarded with the gold particles using a Helios gene gun (Biorad Cat #1652411) pressurized to ~180 psi with helium.

METHOD DETAILS

Molecular cloning—The cDNA for homer1c/PSD-Zip45 was a gift from Shigeo Okabe (University of Tokyo). The PSD95 intrabody was a gift from Don Arnold (USC). PSD95 and GluA1 cDNAs were gifts from Michael Ehlers (Biogen, Inc.). Constructs were generated using standard cloning techniques in a custom chick beta-actin promoter (pCAG) mammalian expression vector. GluA1 constructs were generated by cloning mCh-GluA1 or mOr2-GluA1 into a custom pCAG or pCaMKII promoter backbone containing CIB using PCR to amplify the open reading frame and to remove the stop codon. A second version of this construct was made with mCh and CIB at the C-terminus of GluA1 (GluA1-mCh-CIB), leaving the N-terminus unmodified. This version of the receptor showed no obvious difference in trafficking or functional effects following synaptic recruitment. CRY2PHR (a.a. 1–498) and CIB (a.a. 1–170) were used to generate all fusion constructs, with the exception that we used full length CRY2 for the CRY2-GFP-Homer1c plasmid, which displayed better synaptic localization than CRY2-PHR.

Immunofluorescence—Live cell surface labeling was performed for cells expressing mCh-GluA1-CIB with anti-RFP Abcam #167453 (1:1000). Live cell GluA2 surface labeling was performed using anti-GluA2 Millipore mAb397 (1:500). Live cell GluA1 surface labeling was performed with a custom affinity purified antibody against an extracellular epitope on GluA1 (Kennedy et al., 2010b). Cells were incubated with primary antibodies at the reported dilutions for 10 min at room temperature, washed in ACSF and then either fixed with 4% PFA, or labeled with fluorescent-conjugated secondary Fab fragments (Jackson Immunoresearch #115-177-003) for subsequent live cell imaging. Fixed cells stained with anti-RFP or anti-GluA1 were blocked with 10% normal goat serum in PBS and labeled with fluorescent anti-rabbit secondary antibodies.

Microscopy—Live cell imaging of dissociated hippocampal neurons was carried out at 34°C on an Olympus IX71 equipped with a spinning disc scan head (Yokogawa) with a 60x NA1.4 objective. Excitation illumination was delivered from an AOTF controlled laser launch (Andor) and images were collected on a 1024×1024 pixel Andor iXon EM-CCD camera. Data acquisition and analysis were performed with Metamorph (Molecular Devices), Andor IQ and ImageJ software. All quantification was performed on raw images, but some images were expanded, using the smooth function in ImageJ for display only.

PALM/STORM imaging and analysis

Sample Prep: Dissociated hippocampal neurons were grown on #1.5 cover glass. Light treated cells were exposed to a 1 sec pulse of blue light delivered from a custom built 450nm LED array (Tucker et al., 2014) once every minute for 30 min and immediately fixed in 4% paraformaldehyde for 10 minutes, permeabilized with 0.1% Triton-X100 for 10 minutes and blocked in 5% BSA overnight. Dark treated cells were kept in the dark before and during fixation. Cells were stained for PSD95 (Millipore #MAB1596, 1:1000) or GFP (Thermo #A-11122, 1:1000) and Alexa-647 conjugated secondary (Thermo, 1:2000). TetraSpeck beads (Thermo #T7279, 1:1500) were included in the secondary antibody incubation to aid in drift correction post imaging. Cells were post-fixed with 4% paraformaldehyde, washed and imaged in freshly prepared filtered imaging buffer (50 mM Cysteamine hydrochloride, 10% glucose, 0.6 mg/mL Glucose Oxidase from Aspergillus niger, 0.063 mg/mL Catalase from Bovine liver in PBS, pH between 7.5–8.0).

Imaging: PALM/dSTORM imaging was performed on a Zeiss Elyra P.1 TIRF microscope using a Plan Apochromat 63x 1.4 NA Oil DIC objective and a tube lens providing an extra factor of 1.6x magnification. Alexa-647 molecules were ground-state depleted and imaged with a 100mW 642 laser at 100% AOTF transmission. mEos3.2 was imaged using the 200mW 561 laser line at 35% AOTF transmission. Ground-state return of Alexa647 and photo-conversion of mEos3.2 was elicited by continuous illumination with a 50mW 405 laser at 0.01 to 0.1% AOTF transmission. Excitation light was passed through a quad-band dichroic 405/488/561/642; the emission light was filtered through a laser blocking filter (LBF −561/642). This setup allowed for sequential, one-to-one frame interleaving of the two acquisition channels. 10,000 frames with 50ms integration time for each channel were acquired. Images were recorded with an Andor iXon+ EMCCD, image pixel size was 160 nm x,y.

Localization analysis was performed using Zen 2012 software suite (Zeiss), using previously described methods (Betzig et al., 2006). Briefly, the coordinates of single-molecule events were obtained by fitting a 2D-Gaussian function to intensity-peaks in individual frames (intensity to background threshold was set for 6, the fitting window was set to have a diameter of 9 pixels). Single-molecule peaks with overlapping fitting windows were discarded. Driftcorrection was performed using a model-based algorithm in Zen (Zeiss, proprietary). Fidelity of the drift-correction was confirmed by visual inspection of the localizations for the TetraSpeck fiducial markers. Only localizations with an estimated precision (Mortensen et al., 2010; Thompson et al., 2002) of 10–50nm were used in subsequent analyses.

Localization data was imported into VividSTORM (Barna et al., 2016) where PALM/STORM localizations were overlapped and registered with a widefield image of the 488 channel acquired before PALM/STORM imaging. Regions of interest (ROI) were drawn around individual dendritic spines and localizations within the ROI were exported into MATLAB (Mathworks) for further analysis. Density-based cluster analysis (DBSCAN) (Ester et al., 1996; Tran et al., 2013) implementation in the PALMsiever platform (Pengo et al., 2015) was used to define core, clustered PSD95 localizations. The criterion for assigning individual localizations as core PSD points was the presence of a minimum of 25 neighboring localizations within a 100 nm radius. We found these parameters were robust in identifying PSD95 clusters consistent with the size and shape previously described in the literature (MacGillavry et al., 2013; Nair et al., 2013). The delimitation of the boundaries of the PSD95 cluster were determined by using MATLAB boundary function on the points assigned a core designation. A “shrink-factor” of 0.5 was utilized (where 0 gives a convex hull and 1 results in a compact boundary enveloping all points). The “inpolygon” function was utilized to determine which GluA1 localizations lay on or inside this boundary and these were considered PSD-localized. The Matlab script can be found in supplemental information (Data S1).

Electrophysiology—Whole cell voltage clamp recordings were carried out using either dissociated hippocampal neurons (DIV 17–19, for mEPSC measurements) or organotypic hippocampal slices (DIV 9–12 for evoked EPSCs and aEPSCs) using the following extracellular solutions: for dissociated cultures, cells were bathed in (in mM) 10 HEPES, 130 NaCl, 5 KCl, 30 d-glucose, 2 $CaCl^2$ and 1 $MgCl^2$ supplemented with 1 μM TTX and 30 μM bicuculline for mEPSC recordings. For organotypic slices, recordings were carried out in extracellular solution containing (in mM): 119 NaCl, 2.5 KCl, 26 $NaHCO^3$, 1 NaH^2PO4, 11 glucose, 4 $CaCl^2$ and 4 $MgCl^2$, 0.1 picrotoxin (~300 mOsm) equilibrated with 95 O^2/5% CO^2. For aEPSC experiments, recordings were made in ACSF containing 4 mM $MgCl^2$, 1 mM $CaCl^2$ and 4 mM $SrCl^2$. Some experiments were carried out with no added Ca^{2+} and 6 mM $SrCl^2$ with similar results. To dampen recurrent activity, we isolated CA1 from CA3 with a single cut and included 2-chloroadenosine (2.5–5 μM) in the extracellular solution. For both dissociated and organotypic cultures the intracellular solution contained (in mM): 130 cesium methanesulfonate, 3 Na^2ATP, 0.5 Na^3GTP, 0.5 EGTA, 10 phosphocreatine, 5 $MgCl^2$, 2.5 NaCl, 10 HEPES (290–300 mOsm). The pH was adjusted to 7.25 with CsOH. For evoked EPSCs, stimulation was performed using a theta glass electrode or a concentric bipolar electrode (FHC, Bowdoin, ME) positioned in stratum radiatum, ~200 μm from the targeted neuron. Responses were elicited with a 200 μs pulse and the stimulus intensity adjusted (constant current stimulus isolator, WPI) to evoke 50–200pA EPSCs. Data were collected using a multiclamp 700b amplifier and digitized using a National Instruments DAQ board at 10 KHz and filtered at 2 KHz (single pole Bessel filter) and collected with WinLTP software (University of Bristol). For experiments requiring CRY2 activation, we illuminated the preparation using either a 488nm laser (10–20ms pulse) delivered through the objective, or a GFP filter cube (469 ± 22 nm excitation) with a mercury or metal halide light source for 2 sec every 3 min. Note that the light intensity used to image GFP is fully sufficient to activate CRY2, thus phototoxicity has not been a concern with CRY2 (Kennedy et al., 2010a). For glutamate uncaging experiments, we included 2 mM MNI-glutamate in

the bath solution and focally stimulated the preparation using galvanometric mirrors (FRAPPA, Andor technologies) to steer a diffraction-limited 405 nm spot. An AOTF was used to gate a 500 μs pulse of 405 nm light, with the intensity adjusted to trigger an approximately quantal (10–30pA) AMPA receptor current. Intensities ranged from 3–4% of total laser power from a 100mW 405 nm laser that was fiber coupled to a FRAPPA laser scanning unit. We routinely ensured single spine activation by imaging NMDA receptor Ca^{2+} responses in neurons expressing GCaMP6s (addgene clone #40753) in nominally Mg^{2+}-free extracellular solution containing 1μM TTX. Electrophysiology data were collected and analyzed using WinLTP (University of Bristol) and the NeuroMatic package in IGOR Pro (WaveMetrics). Control (dark-treated, or cells expressing control CIB protein) and experimental (light treated) recordings were interleaved. mEPSC traces were blinded and analyzed using Mini Analysis software package (Synaptosoft). For all recordings, cells were excluded from analysis if the series resistance increased by more than 20% and/or grew larger than 25 MΩ). All electrophysiology experiments were replicated at least twice using independent preparations with sample sizes for each experiment determined by the precision of the measurements from independent cells. We found that a minimum of 6 cells yielded acceptable standard error (typically < ±15% of the measured value) for whole cell recording experiments measuring evoked EPSCs and spontaneous mEPSCs.

FM4-64 loading and optical quantal analysis—For FM4-64 experiments, dissociated hippocampal neurons (DIV 17–20) that had been transfected with mCh-GluA1-CIB and CRY2-GFP-homer1c were incubated with 5μM FM4-64 (Molecular Probes/Thermo) for 1–2 min in normal ACSF containing 10μM NBQX and 50μM APV, followed by a 30 sec exposure to ACSF containing 50mM KCl, 5μM FM4-64, 10μM NBQX and 50μM APV (NaCl was reduced to 80mM in this solution to maintain appropriate osmolarity). Cells were returned to normal ACSF containing 10μM NBQX, 5μM FM4-64 and 50μM APV, incubated for 5 min and then washed with ACSF lacking FM4-64 but containing 1mM ADVASEP-7 (Sigma). Cells were then either exposed to blue light or kept in darkness prior to FM4-64 unloading, which was accomplished by treating cells with isosmotic ACSF containing 50mM KCl, 10μM NBQX and 50μM APV. FM4-64 was imaged using 488nm excitation and emission was collected with a far-red long pass filter. Synapses were identified by the apposition of CRY2-GFP-homer1c and FM4-64 signals. Control (dark treated, no synaptic GluA1 translocation) and experimental (light treated, GluA1 recruited to PSD) trials were interleaved.

For optical quantal analysis, dissociated hippocampal neurons were transfected with SEP-GluA1-CIB, CRY2-homer1c (lacking a fluorescent protein tag) and jRGECO1a (Dana et al., 2016). The frequency and amplitude of spontaneous quantal Ca^{2+} transients were measured at individual dendritic spines in the red channel before and 10 min following SEP-GluA1-CIB recruitment to CRY2-homer1c. Imaging was carried out at a rate of 8 frames/sec. Neurons were imaged in ACSF containing 1μM TTX, 2mM Ca^{2+} but lacking Mg^{2+} to relieve NMDA receptor Mg^{2+} block. Quantal Ca^{2+} transients were eliminated when 50μM APV was added to the bath, confirming they arise from NMDA receptor activation. Because we could not directly visualize CRY2-homer1c in this experiment, we confirmed expression by visualizing the recruitment of SEP-GluA1-CIB to dendritic spines following blue light

exposure. Both FM dye unloading and optical quantal analysis experiments were replicated two times, using independent neuronal preparations with the number of cells and synapses analyzed (at least 120 synapses from 6 cells for FM dye unloading and 72 synapses from 8 cells for optical quantal analysis) determined by the precision of the measurements. These sample sizes yielded standard errors that were < ±15% of the measured values.

QUANTIFICATION AND STATISTICAL ANALYSIS

Quantification for imaging experiments was carried out on raw fluorescent images using ImageJ to measure pixel intensities. Background values (estimated by measuring pixel intensities in image regions with no detectable signal) were routinely subtracted. mEPSC data were blinded and amplitude and frequency were manually measured using Mini Analysis software (synaptosoft). EPSC amplitudes were quantified using the Neuromatic package with Igor Pro (Wavemetrics). Whole cell recording data were excluded if the series resistance changed by more than 20%, or became greater than 25 MΩ over the course of the recording. Statistical analysis was carried out using standard statistical packages in Microsoft Excel. “n” values for electrophysiology experiments represent the number of cells recorded from and are reported for each experiment in the corresponding figure legend. In imaging experiments, the definition of n values are specified in figure legends but typically represent the number of synapses from at least 5 different neurons from at least 3 independent cultures. We used Student’s t-test to compare two populations. We used paired Student’s t-tests when values were measured from the same cells or synapses before and after treatment (e.g. exposure to blue light). The statistical tests used are standard and no method was used to validate the specific assumptions of each statistical test. Definition of error bars, statistical tests and p values can be found in corresponding figure legends. Differences were deemed “significant” if the p value comparing the populations using the specified statistical test was less than 0.05.

DATA AND SOFTWARE AVAILABILITY

The Custom Matlab script for defining the PSD boundary from our PALM/STORM localization data and the AMPA receptor occupancy within this boundary is included as a downloadable file (Data S1).

ADDITIONAL RESOURCES

Plasmids from this study will be made available through Addgene.

Supplementary Material

Refer to Web version on PubMed Central for supplementary material.

Acknowledgments

We would like to Acknowledge Drs. Jason Aoto, Tim Benke, Paco Herson, Abigail Person and Chandra Tucker for critical discussions and Radu Moldovan from the Advanced Light Microscopy Core Facility at the University of Colorado School of Medicine. This work was supported by T32AA007464 (K.C.C), T32HD041697 (J.S.F.), NS040701 (M.L.D.),T32GM007635 (B.L.S), NS092421 (A.B.B) and NS082271, The McKnight Foundation, The Pew Charitable Trusts, The Brain Research Foundation, The Brain and Behavior Research Foundation and The Boettcher Foundation (M.J.K).

References

Bagal AA, Kao JP, Tang CM, Thompson SM. Long-term potentiation of exogenous glutamate responses at single dendritic spines. Proc Natl Acad Sci U S A. 2005; 102:14434–14439. [PubMed: 16186507]

Banke TG, Bowie D, Lee HK, Huganir RL, Schousboe A, Traynelis SF. Control of GluR1 AMPA Receptor Function by cAMP-Dependent Protein Kinase. J Neurosci. 2000; 20:89–102. [PubMed: 10627585]

Barna L, Dudok B, Miczán V, Horváth A, László ZI, Katona I. Correlated confocal and super-resolution imaging by VividSTORM. Nat Protoc. 2016; 11:163–183. [PubMed: 26716705]

Bekkers JM, Clements JD. Quantal amplitude and quantal variance of strontium-induced asynchronous EPSCs in rat dentate granule neurons. J Physiol. 1999; 516:227–248. [PubMed: 10066937]

Benke TA, Luthi A, Isaac JT, Collingridge GL. Modulation of AMPA receptor unitary conductance by synaptic activity. Nature. 1998; 393:793–797. [PubMed: 9655394]

Betzig E, Patterson GH, Sougrat R, Lindwasser OW, Olenych S, Bonifacino JS, Davidson MW, Lippincott-Schwartz J, Hess HF. Imaging intracellular fluorescent proteins at nanometer resolution. Science. 2006; 313:1642–1645. [PubMed: 16902090]

Bingol B, Schuman EM. Activity-dependent dynamics and sequestration of proteasomes in dendritic spines. Nature. 2006; 441:1144–1148. [PubMed: 16810255]

Blanpied TA, Scott DB, Ehlers MD. Dynamics and regulation of clathrin coats at specialized endocytic zones of dendrites and spines. Neuron. 2002; 36:435–49. [PubMed: 12408846]

Bosch M, Castro J, Saneyoshi T, Matsuno H, Sur M, Hayashi Y. Structural and molecular remodeling of dendritic spine substructures during long-term potentiation. Neuron. 2014; 82:444–459. [PubMed: 24742465]

Boyden ES, Zhang F, Bamberg E, Nagel G, Deisseroth K. Millisecond-timescale, genetically targeted optical control of neural activity. Nat Neurosci. 2005; 8:1263–1268. [PubMed: 16116447]

Chen TW, Wardill TJ, Sun Y, Pulver SR, Renninger SL, Baohan A, Schreiter ER, Kerr RA, Orger MB, Jayaraman V, Looger LL, Svoboda K, Kim DS. Ultrasensitive fluorescent proteins for imaging neuronal activity. Nature. 2013; 499:295–300. [PubMed: 23868258]

Dana H, Mohar B, Sun Y, Narayan S, Gordus A, Hasseman JP, Tsegaye G, Holt GT, Hu A, Walpita D, et al. Sensitive red protein calcium indicators for imaging neural activity. Elife. 2016; 5

Dani A, Huang B, Bergan J, Dulac C, Zhuang X. Superresolution imaging of chemical synapses in the brain. Neuron. 2010; 68:843–856. [PubMed: 21144999]

Durand GM, Kovalchuk Y, Konnerth A. Long-term potentiation and functional synapse induction in developing hippocampus. Nature. 1996; 381:71–75. [PubMed: 8609991]

Ester, M., Kriegel, H-P., Sander, J., Xu, X. A Density-Based Algorithm for Discovering Clusters in Large Spatial Databases with Noise. Proc. 2nd Int. Conf. KDD; 1996. p. 1232-1239.

Fitzjohn S, Pickard L, Duckworth J, Molnar E, Henley J, Collingridge G, Noël J. An electrophysiological characterisation of long-term potentiation in cultured dissociated hippocampal neurones. Neuropharmacology. 2001; 41:693–699. [PubMed: 11640923]

Franks KM, Stevens CF, Sejnowski TJ. Independent sources of quantal variability at single glutamatergic synapses. J Neurosci. 2003; 23:3186–3195. [PubMed: 12716926]

Granger AJ, Shi Y, Lu W, Cerpas M, Nicoll RA. LTP requires a reserve pool of glutamate receptors independent of subtype. Nature. 2013; 493:495–500. [PubMed: 23235828]

Gross GG, Junge JA, Mora RJ, Kwon HB, Olson CA, Takahashi TT, Liman ER, Ellis-Davies GCR, McGee AW, Sabatini BL, et al. Recombinant probes for visualizing endogenous synaptic proteins in living neurons. Neuron. 2013; 78:971–985. [PubMed: 23791193]

Gu J, Lee CW, Fan Y, Komlos D, Tang X, Sun C, Yu K, Hartzell HC, Chen G, Bamburg JR, et al. ADF/cofilin-mediated actin dynamics regulate AMPA receptor trafficking during synaptic plasticity. Nat Neurosci. 2010; 13:1208–1215. [PubMed: 20835250]

Halt AR, Dallapiazza RF, Zhou Y, Stein IS, Qian H, Juntti S, Wojcik S, Brose N, Silva AJ, Hell JW. CaMKII binding to GluN2B is critical during memory consolidation. EMBO J. 2012; 31:1203–1216. [PubMed: 22234183]

Hayashi Y, Shi SH, Esteban JA, Piccini A, Poncer JC, Malinow R. Driving AMPA receptors into synapses by LTP and CaMKII: requirement for GluR1 and PDZ domain interaction. Science. 2000; 287:2262–2267. [PubMed: 10731148]

Heilemann M, van de Linde S, Schüttpelz M, Kasper R, Seefeldt B, Mukherjee A, Tinnefeld P, Sauer M. Subdiffraction-resolution fluorescence imaging with conventional fluorescent probes. Angew Chem Int Ed Engl. 2008; 47:6172–6176. [PubMed: 18646237]

Isaac JT, Nicoll RA, Malenka RC. Evidence for silent synapses: implications for the expression of LTP. Neuron. 1995; 15:427–434. [PubMed: 7646894]

Kauer JA, Malenka RC, Nicoll RA. A persistent postsynaptic modification mediates long-term potentiation in the hippocampus. Neuron. 1988; 1:911–917. [PubMed: 2908443]

Keith DJ, Sanderson JL, Gibson ES, Woolfrey KM, Robertson HR, Olszewski K, Kang R, El-Husseini A, Dell'acqua ML. Palmitoylation of A-kinase anchoring protein 79/150 regulates dendritic endosomal targeting and synaptic plasticity mechanisms. J Neurosci. 2012:7119–7136. [PubMed: 22623657]

Kennedy MJ, Hughes RM, Peteya LA, Schwartz JW, Ehlers MD, Tucker CL. Rapid blue-light-mediated induction of protein interactions in living cells. Nat Methods. 2010a; 7:973–975. [PubMed: 21037589]

Kennedy MJ, Davison IG, Robinson CG, Ehlers MD. Syntaxin-4 Defines a Domain for Activity-Dependent Exocytosis in Dendritic Spines. Cell. 2010b; 141:524–535. [PubMed: 20434989]

Kerchner GA, Nicoll RA. Silent synapses and the emergence of a postsynaptic mechanism for LTP. Nat Rev Neurosci. 2008; 9:813–825. [PubMed: 18854855]

Kuriu T, Inoue A, Bito H, Sobue K, Okabe S. Differential control of postsynaptic density scaffolds via actin-dependent and -independent mechanisms. J Neurosci. 2006; 26:7693–706. [PubMed: 16855097]

Liao D, Hessler NA, Malinow R. Activation of postsynaptically silent synapses during pairing-induced LTP in CA1 region of hippocampal slice. Nature. 1995; 375:400–404. [PubMed: 7760933]

Lindskog M, Li L, Groth RD, Poburko D, Thiagarajan TC, Han X, Tsien RW. Postsynaptic GluA1 enables acute retrograde enhancement of presynaptic function to coordinate adaptation to synaptic inactivity. Proc Natl Acad Sci U S A. 2010; 107:21806–21811. [PubMed: 21098665]

Lisman J, Raghavachari S. A unified model of the presynaptic and postsynaptic changes during LTP at CA1 synapses. Sci STKE. 2006; 2006:re11. [PubMed: 17033044]

Lu W, Man H, Ju W, Trimble WS, MacDonald JF, Wang YT. Activation of synaptic NMDA receptors induces membrane insertion of new AMPA receptors and LTP in cultured hippocampal neurons. Neuron. 2001; 29:243–254. [PubMed: 11182095]

Lu W, Shi Y, Jackson AC, Bjorgan K, During MJ, Sprengel R, Seeburg PH, Nicoll RA. Subunit composition of synaptic AMPA receptors revealed by a single-cell genetic approach. Neuron. 2009; 62:254–268. [PubMed: 19409270]

Luscher C, Nicoll RA, Malenka RC, Muller D. Synaptic plasticity and dynamic modulation of the postsynaptic membrane. Nat Neurosci. 2000; 3:545–550. [PubMed: 10816309]

MacGillavry HD, Song Y, Raghavachari S, Blanpied TA. Nanoscale scaffolding domains within the postsynaptic density concentrate synaptic AMPA receptors. Neuron. 2013; 78:615–622. [PubMed: 23719161]

Malgaroli A, Tsien RW. Glutamate-induced long-term potentiation of the frequency of miniature synaptic currents in cultured hippocampal neurons. Nature. 1992; 357:134–139. [PubMed: 1349728]

Malinow R, Tsien RW. Presynaptic enhancement shown by whole-cell recordings of long-term potentiation in hippocampal slices. Nature. 1990; 346:177–180. [PubMed: 2164158]

Matsuzaki M, Honkura N, Ellis-Davies GC, Kasai H. Structural basis of long-term potentiation in single dendritic spines. Nature. 2004; 429:761–766. [PubMed: 15190253]

McAllister AK, Stevens CF. Nonsaturation of AMPA and NMDA receptors at hippocampal synapses. Proc Natl Acad Sci U S A. 2000; 97:6173–6178. [PubMed: 10811899]

Meng Y, Zhang Y, Jia Z. Synaptic transmission and plasticity in the absence of AMPA glutamate receptor GluR2 and GluR3. Neuron. 2003; 39:163–176. [PubMed: 12848940]

Mortensen KI, Churchman LS, Spudich JA, Flyvbjerg H. Optimized localization analysis for single-molecule tracking and super-resolution microscopy. Nat Methods. 2010; 7:377–381. [PubMed: 20364147]

Nair D, Hosy E, Petersen JD, Constals A, Giannone G, Choquet D, Sibarita JB. Super-Resolution Imaging Reveals That AMPA Receptors Inside Synapses Are Dynamically Organized in Nanodomains Regulated by PSD95. J Neurosci. 2013; 33:13204–13224. [PubMed: 23926273]

O'Brien RJ, Kamboj S, Ehlers MD, Rosen KR, Fischbach GD, Huganir RL. Activity-dependent modulation of synaptic AMPA receptor accumulation. Neuron. 1998; 21:1067–1078. [PubMed: 9856462]

Opazo P, Sainlos M, Choquet D. Regulation of AMPA receptor surface diffusion by PSD-95 slots. Curr Opin Neurobiol. 2012; 22:453–460. [PubMed: 22051694]

Pengo T, Holden SJ, Manley S. PALMsiever: a tool to turn raw data into results for single-molecule localization microscopy. Bioinformatics. 2015; 31:797–798. [PubMed: 25362091]

Raghavachari S, Lisman JE. Properties of quantal transmission at CA1 synapses. J Neurophysiol. 2004; 92:2456–2467. [PubMed: 15115789]

Redondo RL, Morris RG. Making memories last: the synaptic tagging and capture hypothesis. Nat Rev Neurosci. 2011; 12:17–30. [PubMed: 21170072]

Ripley B, Otto S, Tiglio K, Williams ME, Ghosh A. Regulation of synaptic stability by AMPA receptor reverse signaling. Proc Natl Acad Sci U S A. 2011; 108:367–372. [PubMed: 21173224]

Rust MJ, Bates M, Zhuang X. Sub-diffraction-limit imaging by stochastic optical reconstruction microscopy (STORM). Nat Methods. 2006; 3:793–795. [PubMed: 16896339]

Sanderson JL, Gorski JA, Gibson ES, Lam P, Freund RK, Chick WS, Dell'Acqua ML. AKAP150-anchored calcineurin regulates synaptic plasticity by limiting synaptic incorporation of Ca2+-permeable AMPA receptors. J Neurosci. 2012; 32:15036–15052. [PubMed: 23100425]

Shen K, Meyer T. Dynamic control of CaMKII translocation and localization in hippocampal neurons by NMDA receptor stimulation. Science. 1999; 284:162–166. [PubMed: 10102820]

Shi SH, Hayashi Y, Petralia RS, Zaman SH, Wenthold RJ, Svoboda K, Malinow R. Rapid spine delivery and redistribution of AMPA receptors after synaptic NMDA receptor activation. Science. 1999; 284:1811–1816. [PubMed: 10364548]

Sinnen BL, Bowen AB, Gibson ES, Kennedy MJ. Local and Use-Dependent Effects of β-amyloid Oligomers on NMDA Receptor Function Revealed by Optical Quantal Analysis. J Neurosci. 2016; 36:11532–43. [PubMed: 27911757]

Spencer DM, Wandless TJ, Schreiber SL, Crabtree GR. Controlling signal transduction with synthetic ligands. Science. 1993; 262:1019–1024. [PubMed: 7694365]

Stoppini L, Buchs PA, Muller D. A simple method for organotypic cultures of nervous tissue. J Neurosci Methods. 1991; 37:173–182. [PubMed: 1715499]

Tang AH, Chen H, Li TP, Metzbower SR, MacGillavry HD, Blanpied TA. A trans-synaptic nanocolumn aligns neurotransmitter release to receptors. Nature. 2016; 536:210–214. [PubMed: 27462810]

Thompson RE, Larson DR, Webb WW. Precise nanometer localization analysis for individual fluorescent probes. Biophys J. 2002; 82:2775–2783. [PubMed: 11964263]

Tracy TE, Yan JJ, Chen L. Acute knockdown of AMPA receptors reveals a trans-synaptic signal for presynaptic maturation. EMBO J. 2011; 30:1577–1592. [PubMed: 21378752]

Tran TN, Drab K, Daszykowski M. Revised DBSCAN algorithm to cluster data with dense adjacent clusters. Chemom Intell Lab Syst. 2013; 120:92–96.

Tucker CL, Vrana JD, Kennedy MJ. Tools for controlling protein interactions using light. Curr Protoc Cell Biol. 2014; 64:17.16.1–20.

Turrigiano GG, Leslie KR, Desai NS, Rutherford LC, Nelson SB. Activity-dependent scaling of quantal amplitude in neocortical neurons. Nature. 1998; 391:892–896. [PubMed: 9495341]

Yang Y, Wang XB, Frerking M, Zhou Q. Delivery of AMPA receptors to perisynaptic sites precedes the full expression of long-term potentiation. Proc Natl Acad Sci U S A. 2008; 105:11388–11393. [PubMed: 18682558]

Woods G, Zito K. Preparation of gene gun bullets and biolistic transfection of neurons in slice culture. J Vis Exp. 2008

Zhang YPP, Holbro N, Oertner TG. Optical induction of plasticity at single synapses reveals input-specific accumulation of alphaCaMKII. Proc Natl Acad Sci U S A. 2008; 105:12039–12044. [PubMed: 18697934]

Highlights

- A new method for rapidly and locally tuning the level of synaptic proteins in the PSD
- Adding AMPA receptors to the PSD elevated quantal frequency, amplitude was unaffected
- Data support the presence of “silent synapses” that contain few or no AMPA receptors
- Functional subdomains within the PSD limit quantal amplitude

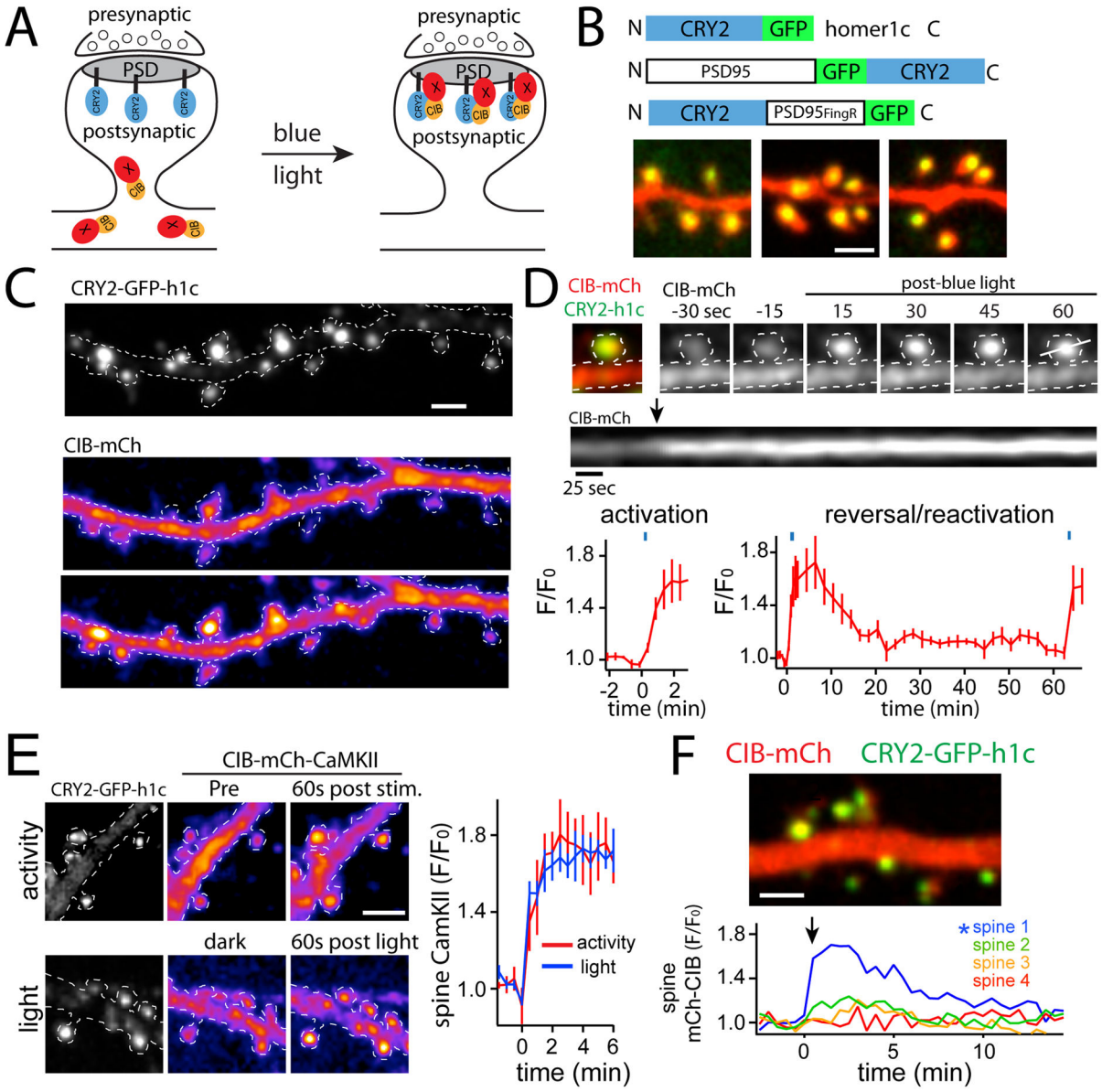

Figure 1. Optogenetic approach for controlling the molecular composition of the excitatory postsynaptic membrane

A. Schematic of synaptic recruitment strategy. CRY2 is localized to the PSD by fusing it to a PSD scaffold molecule. Light activates CRY2 to bind CIB-fused proteins, allowing conditional recruitment to the postsynaptic membrane.

B. Schematic of CRY2 scaffold proteins used in this study. CRY2-fused homer1c, PSD95 and a genetically encoded “intrabody” that binds to endogenous PSD95 ($PSD95_{FingR}$) localize to dendritic spines (arrowheads). Scale bar 1.5 μm.

C. Soluble CIB-mCh is rapidly recruited to synapses by blue light activation. Top panel, CRY2-GFP-homer1c, middle panel CIB-mCh prior to light exposure, bottom panel CIB-mCh 2 min following exposure to blue light. Scale bar 2 μm.

D. Kinetics and reversibility of optical translocation using CRY2. Shown is a spine from a dissociated hippocampal neuron expressing CRY2-GFP-homer1c (green) and CIB-mCh (red). Light triggers rapid accumulation of CIB-mCh within dendritic spines. The kymograph below was generated using the white line in the last panel. The graphs plot the kinetics of CIB-mCh synaptic recruitment (left panel) and dissociation (right panel) following a single 50ms blue light exposure (488nm). CRY2 can be re-activated with a subsequent light pulse. The timing of light exposure is given by the blue dashes above the plots.

E. CRY2-induced PSD recruitment occurs with similar kinetics and magnitude to molecular translocations induced by synaptic activity. Recruitment of CIB-mCh-CaMKII by light (bottom panels) and synaptic activity triggered by cLTP (top panels). Scale bar 2 μm. The kinetics of CIB34 mCh-CaMKII spine accumulation in response to light or activity are plotted. n=20 spines from 3 neurons for each condition (±SEM).

F. Individual synapses can be modified using CRY2/CIB dimerization. Spine 1 was photostimulated with a 1 ms pulse of diffraction-limited 488nm light. Recruitment of CIB-mCh is quantified (bottom panel) at the photostimulated spine (asterisk) and closely neighboring spines (spines 2–4). Scale bar 2 μm. See also Movie S1.

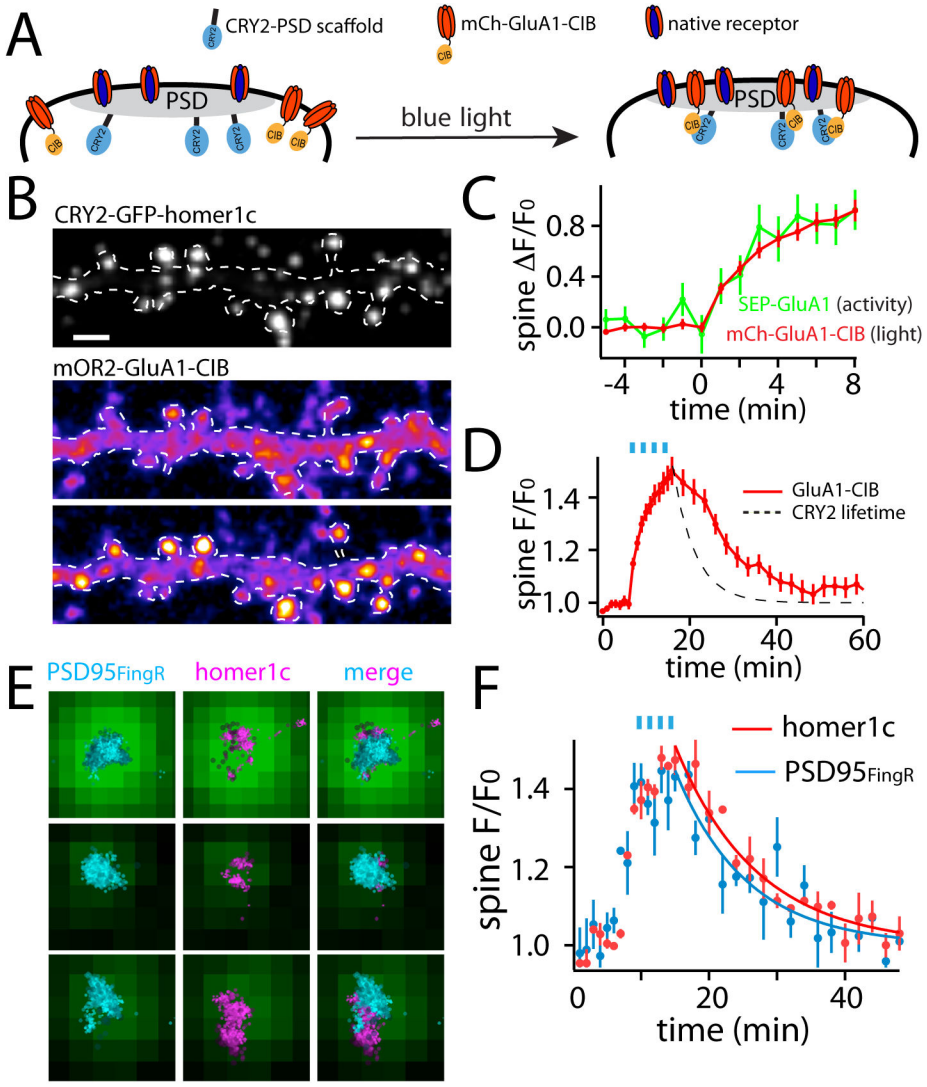

Figure 2. Optical recruitment of AMPA receptors to synapses

A. Schematic for AMPA receptor recruitment to the PSD of excitatory synapses.

B. Shown is a dendrite from a live dissociated hippocampal neuron expressing CRY2-GFP-homer1c (top panel) along with mOR2-GluA1-CIB before (middle panel) and 5 min after (bottom panel) blue light treatment. Note the robust enrichment of mOR2-GluA1-CIB in dendritic spines following light exposure (arrowheads). Scale bar 2 μm. See also Fig. S1, Movie S2.

C. Light-triggered GluA1-CIB synaptic translocation (red line) is plotted along with cLTP-induced SEP-GluA1 synaptic accumulation (green line).

D. Kinetics and reversibility of GluA1 translocation. Hippocampal neurons expressing CRY2-GFP-homer1c along with GluA1-mCh-CIB were treated with blue light to drive AMPA receptors into synapses and imaged for an additional 40 min to measure reversibility. Mean values from 59 spines from 6 neurons are plotted ±SEM. The dashed line represents the lifetime of the CRY2/CIB interaction.

E. PALM/dSTORM images of endogenous PSD95 (mEOS-PSD95$_{FingR}$; teal) and expressed CRY2-GFPhomer1c (magenta, detected with anti-GFP and Alexa-647). The epifluorescent GFP signal from CRY2-GFP-homer1c is shown in green. The dimension of each image is 1.3 × 1.3μm. Localization precision values (mean±standard deviation) are 25.1±9.8nm (GFP-homer1c/Alexa-647) and 23.7±10.1nm (PSD95$_{FingR}$-mEOS).

F. Kinetics of light-triggered accumulation and dissociation of GluA1-mCh-CIB measured in spines from neurons expressing either CRY2-GFP-homer1c (red) or CRY2-PSD95$_{FingR}$ (blue). The data were fit with a single exponential decay function (solid lines). Mean values are plotted ±SEM.

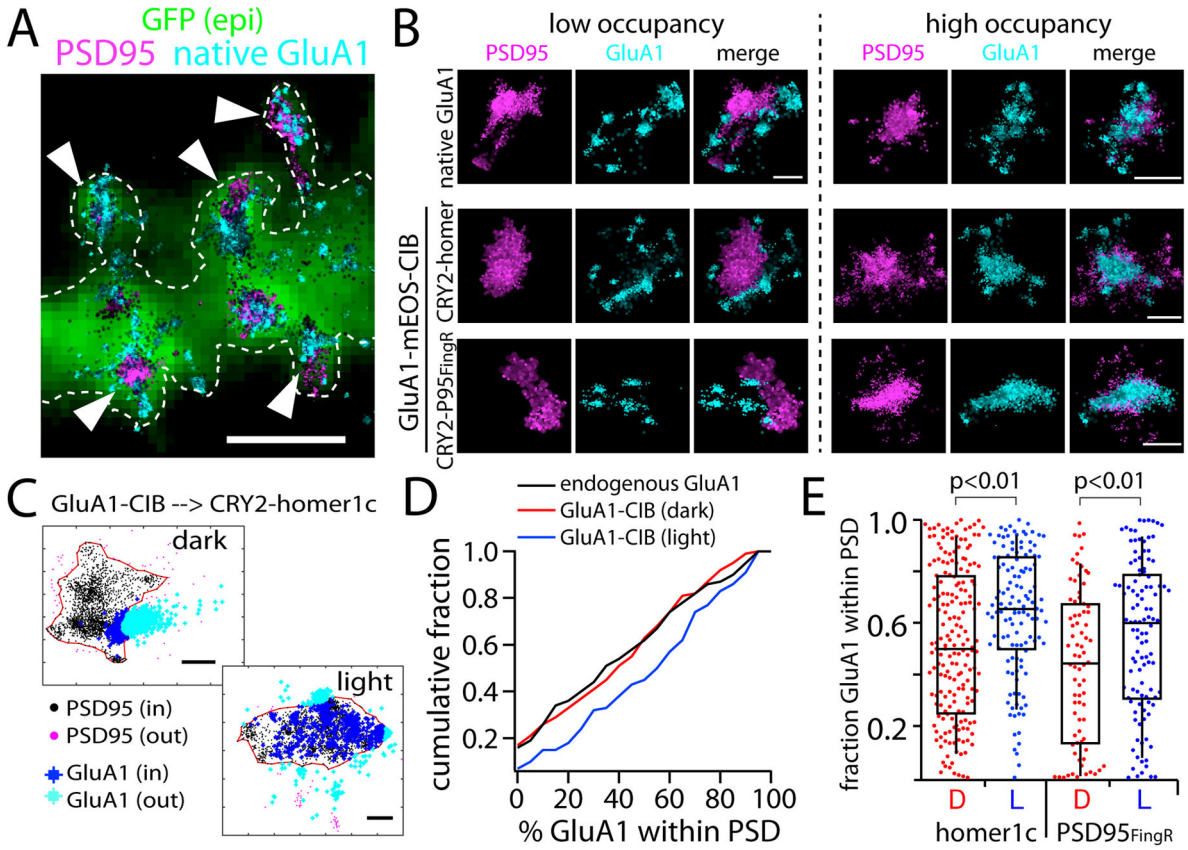

Figure 3. Recruited GluA1 infiltrates the postsynaptic density

A. Representative PALM/STORM image showing endogenous surface GluA1 detected with an antibody (teal) along with endogenous PSD95 detected with mEOS-PSD95$_{FingR}$ (magenta). Arrowheads denote spine synapses. Scale bar 2.2 μm.

B. Endogenous GluA1 (teal, top row) or expressed GluA1-mEOS-CIB (teal, bottom two rows) at individual synapses displayed a wide range of overlap with the PSD, defined by endogenous PSD95 staining (magenta). Representative low- (left) and high-overlap (right) examples are shown. Scale bars 500nm.

C. Method for calculating the fraction of PSD-localized GluA1 within individual spines. Shown are individual localization points from PALM/STORM images of GluA1-mEOS-CIB and antibody-labeled endogenous PSD95. A polygon region based on a minimum density of PSD95 localizations was automatically generated for each dendritic spine to define the PSD boundary. GluA1-mEOS-CIB localizations within the PSD boundary were divided by the total number of spine localizations to calculate fractional PSD occupancy. Scale bar 200 nm. Localization precision values (mean±standard deviation) are 26.0±8.8 (PSD95/Alexa-647) and 20.1±8.5nm (GluA1-mEOS).

D. The cumulative distribution of GluA1 synaptic localization (expressed as fraction within the PSD) is plotted for endogenous GluA1 (black, 122 spines from 6 cells), expressed GluA1-mEOS-CIB in dark-treated cells (red, 79 spines from 6 cells) and expressed GluA1-mEOS-CIB recruited to CRY2-PSD95$_{FingR}$ in light-treated cells (blue, 111 spines from 6

cells). Endogenous GluA1 vs. GluA1-CIB dark n.s.; GluA1-CIB, dark vs GluA1-CIB light $p<0.01$; endogenous GluA1 vs GluA1-CIB light $p<0.01$, Student's t-test.

E. Scatter plots of the fraction of PSD-localized GluA1 in dark and light-treated neurons expressing GluA1-CIB along with either CRY2-homer1c or CRY2-PSD95$_{FingR}$. The box represents the median, upper and lower quartile of the distribution and the whiskers extend to the top and bottom 10th percentiles. Homer dark, 197 spines from 6 neurons; homer light, 127 spines from 6 neurons; PSD95$_{FingR}$ light, 111 spines from 6 neurons; PSD95$_{FingR}$ dark, 79 spines from 6 neurons. $p<0.01$, Student's t-test comparing light to dark conditions for both CRY2-PSD95$_{FingR}$ and CRY2-homer1c.

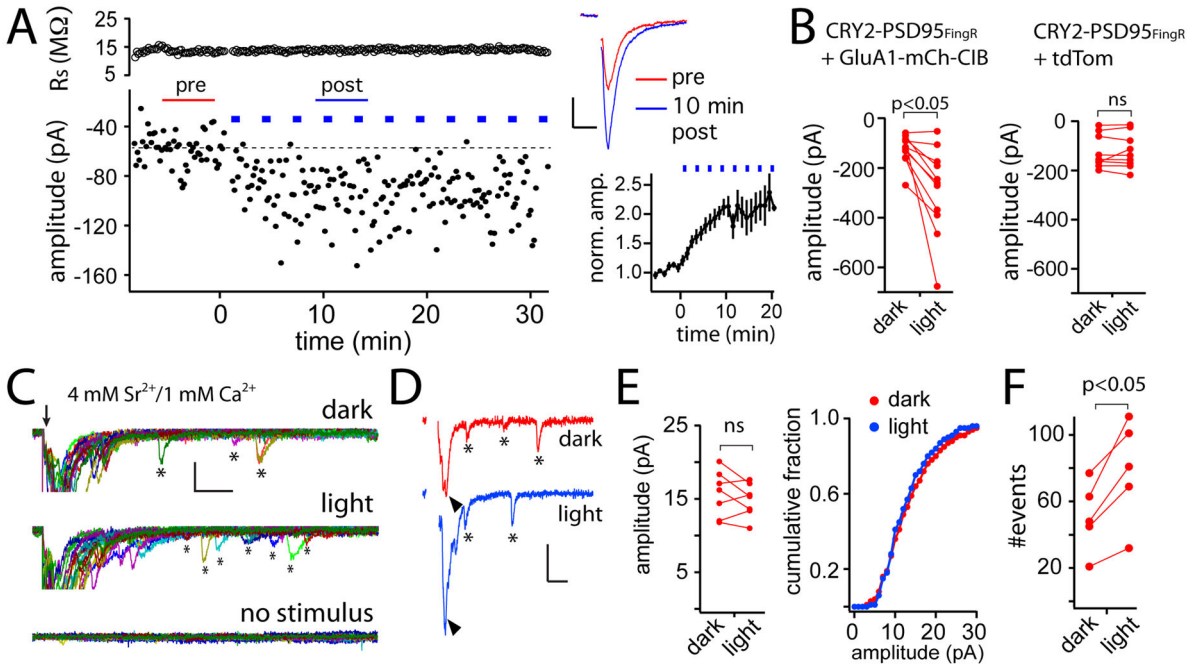

Figure 4. GluA1 recruitment to the PSD results in functional enhancement of excitatory neurotransmission

A. Shown is a representative experiment measuring whole cell evoked EPSC amplitudes from a CA1 pyramidal neuron in an organotypic hippocampal slice expressing CRY2-PSD95$_{FingR}$ along with GluA1-mCh-CIB before and after blue light exposure. Series resistance is plotted above. Averaged (30 sweeps) dark (red) and post-light (blue) traces are shown to the right. The stimulus artifact has been removed for clarity. Scale bar 20pA/20ms. The lower-right graph shows the kinetics of EPSC potentiation averaged from 11 different cells (±SEM).

B. Evoked EPSC amplitudes were measured as in (A) before and 20 min following light exposure for 11 cells expressing CRY2-PSD95$_{FingR}$ and GluA1-mCh-CIB (left panel, p= 0.01 paired Student's t-test) or 9 control cells expressing CRY2-PSD95$_{FingR}$ and tdTom (right panel p= 0.75, paired Student's t-test).

C. Asynchronous evoked release events were measured from CA1 pyramidal cells in organotypic hippocampal slices expressing CRY2-PSD95$_{FingR}$ along with GluA1-mCh-CIB. ACSF contained 1 mM Ca^{2+} and 4 mM Sr^{2+}. Twenty sweeps (stimulus delivered at arrow) are shown from the same cell before (top traces) and 20 min following blue light exposure (middle traces). Bottom traces show control sweeps with no stimulus. Putative quantal events are marked with asterisks. Scale bar 40 pA/25 ms.

D. Representative asynchronous release traces before and after blue light. Note the increased size of the evoked EPSC (arrowheads), but similar sized aEPSCs (asterisks) before and after light treatment. The stimulus artifacts have been removed for clarity. Scale bar 50 pA/25 ms.

E. Mean aEPSC amplitudes are plotted for 7 different cells before and after blue light treatment (left plot). The right plot shows the cumulative distribution of aEPSC amplitudes (n=548 events dark, 548 events light, from 7 cells) before (red) and 15–20 min after (blue) light exposure (p=0.42, Kolmogorov-Smirnov test).

F. The total number of aEPSCs were counted in a time window 50 to 200 ms following stimulation for 50 consecutive sweeps before and after blue light exposure for 5 cells ($p<0.05$ paired, Students t-test).

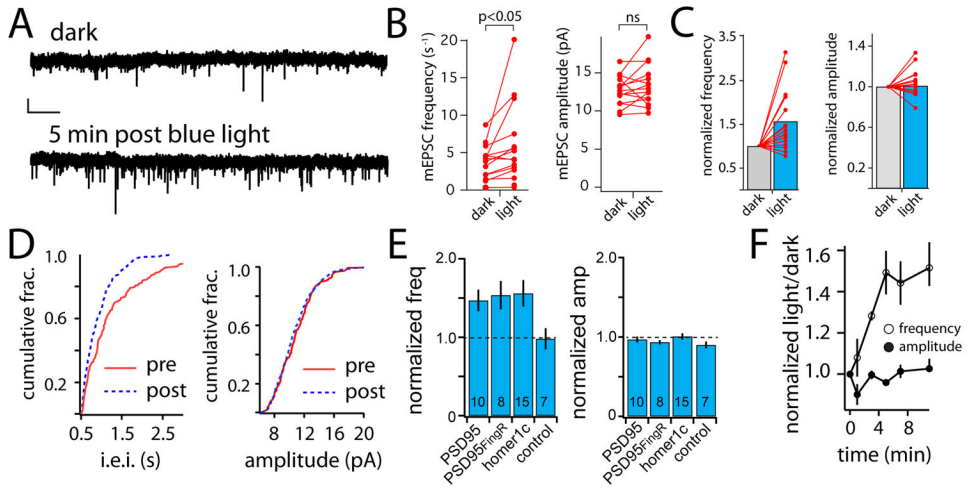

Figure 5. Recruitment of AMPA receptors to the PSD increases quantal frequency but not amplitude

A. mEPSCs were measured from the same dissociated hippocampal neuron (expressing GluA1-mCh-CIB and CRY2-GFP-homer1c) in the dark and 5 min following blue light exposure. Scale bar 10 pA/1 s.

B. mEPSC amplitude and frequency values measured in the dark and 6–8 min following blue light are plotted for dissociated hippocampal neurons expressing GluA1-mCh-CIB along with CRY2-GFP-homer1c (n=14 cells, frequency dark vs light, p= 0.028, amplitude dark vs light p= 0.18, paired Student's t-test).

C. mEPSC amplitude and frequency normalized to their respective dark values are shown.

D. Cumulative distributions (250 events) of mEPSC frequency (inter-event interval, left panel) and amplitude (right panel) for a representative neuron expressing CRY2-GFP-homer1c and GluA1-mCh-CIB in the dark (red) and 6–8 min following light exposure (blue). Note the robust decrease in inter-event interval (p=0.004, Kolmogorov-Smirnov test), with no significant change in amplitude (p= 0.695, Kolmogorov-Smirnov test).

E. Normalized mEPSC frequency (left panel) and amplitude (right panel) values are plotted for cells where GluA1-mCh-CIB was recruited to different PSD scaffolds: PSD95-GFP-CRY2, CRY2-GFPPSD95$_{FingR}$ or CRY2-GFP-homer1c. Control cells expressed CRY2-GFP-homer1c and CIB-mCh instead of GluA1-mCh-CIB. mEPSC frequency and amplitude values were measured 6–8 min following light exposure and normalized to their respective dark baseline values. The number on each bar represents the number of cells recorded for each condition, ±SEM.

F. Average mEPSC frequency (open circles) and amplitude (filled circles) values (normalized to dark baseline values) are plotted as a function of time after blue light onset. mCh-GluA1-CIB was recruited to CRY2-GFP-homer1c for this experiment. Values represent averages from 6 neurons ±SEM. See also Fig. S2.

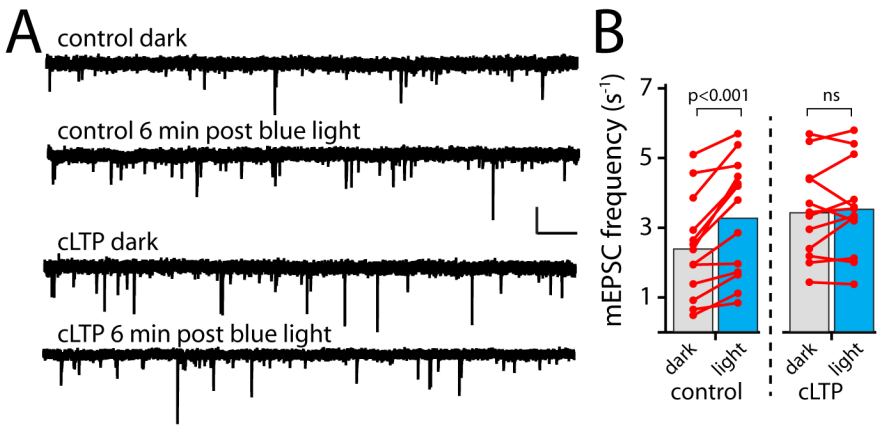

Figure 6. LTP stimulus occludes AMPA receptor functional incorporation

A. Shown are mEPSC recordings from primary hippocampal neurons expressing CRY2-homer1c and GluA1-mCh-CIB. Traces are from the same cells in darkness and 6 min following blue light exposure for a control cell (top traces) and a cell pre-treated with cLTP stimulus (bottom traces). Scale bar 20pA, 1 sec.

B. cLTP occludes light triggered changes in mEPSC frequency (control dark vs. light, $p<0.001$ paired Student's t-test, n=13 neurons; cLTP dark vs. light $p=0.55$, paired Student's t-test, n=12 neurons). See also Fig. S3.

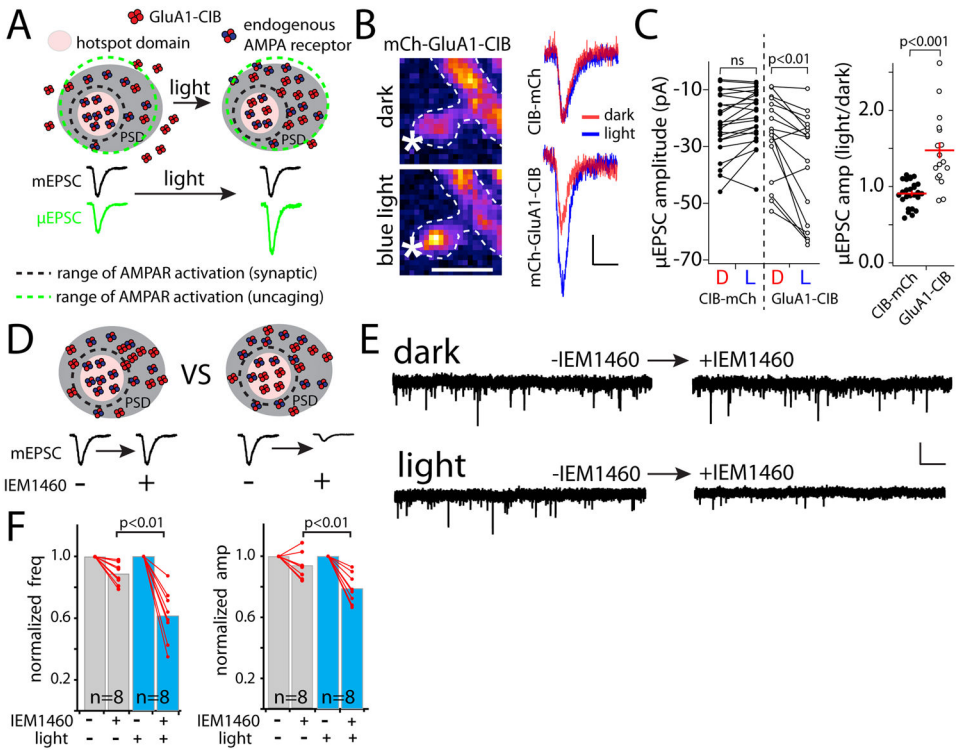

Figure 7. Functional evidence for synaptic organization of AMPA receptors

A. Model for lack of increase in quantal amplitude upon receptor recruitment. En face view of a PSD showing a hotspot domain (pink circle) that clusters AMPA receptors near presynaptic release sites. The black dashed line represents the radius of glutamate required for effective AMPA receptor activation, centered on a vesicular release site. Quantal AMPA responses are determined by the density of receptors within the hotspot. Enlarging the radius of receptor activation (green dashed line represents radius of AMPA receptor activation by MNI-glutamate uncaging) will activate an expanded pool of receptors within the PSD.

B. AMPA receptor currents were measured in response to single spine MNI-glutamate uncaging before (top panel) and after (bottom panel) GluA1-CIB recruitment. Averaged (3 sweeps) μEPSCs recorded before (red) and 5 min following (blue) light exposure are shown to the right for neurons expressing CRY2-homer1c along with either CIB-mCh (top) or mCh-GluA1-CIB. Scale bars for image, 1μm; recordings, 10pA/20msec.

C. Paired plots showing dark baseline (D) and post-light (L) μEPSC amplitude values for control cells expressing CIB-mCh (left, filled circles) and for cells expressing mCh-GluA1-CIB (right, open circles) (GluA1-CIB, n=17 spines from 6 neurons, $p<0.01$; CIB-mCh, n=26 spines from 6 neurons n.s. paired Student's t-test). Normalized (post-light values divided by dark values) data are plotted in the graph to the right.

D. Two models to explain the lack of increase in quantal amplitude upon GluA1 recruitment: GluA1 receptors cannot functionally integrate into established functional domains within the PSD (left) or they are in equilibrium with endogenous AMPA receptors in functional domains (right). These possibilities can be distinguished using IEM1460, which selectively blocks expressed homomeric GluA1-CIB receptors. Legend in (A) also applies here.

E. Representative mEPSC recordings from neurons expressing mCh-GluA1-CIB and CRY2-homer1c before (left traces) and 5 min after (right traces) adding 50 μM IEM1460. Neurons were either pre-treated with light (bottom traces) or kept in the dark (top traces). Scale bar 20 pA/1 sec.

F. Normalized (post-IEM1460 values divided by pre-IEM1460 values) mEPSC frequency (left panel) and amplitude (right panel) are plotted for cells either kept in the dark (n=8 cells, grey bars), or pre-treated with light (n=8 cells, blue bars); $p<0.001$ (frequency), $p>0.01$ (amplitude), Student's t-test. See also Fig. S4.